

UNIVERSIDADE FEDERAL DO RIO GRANDE DO SUL
INSTITUTO DE FÍSICA
DEPARTAMENTO DE ASTRONOMIA

Pode ω Centauri induzir formação estelar no disco Galáctico?*

Gustavo Malta Salerno, Bel., Lic.

Dissertação realizada sob orientação do Professor Dr. Eduardo Luiz Damiani Bica e apresentada ao Programa de Pós-Graduação do Instituto de Física da UFRGS em preenchimento parcial dos requisitos para a obtenção do título de Mestre em Física.

Porto Alegre

Agosto, 2013

*Trabalho parcialmente financiado pelo Conselho Nacional de Desenvolvimento Científico e Tecnológico (CNPq).

Para Ota, Mãozinha, Manetinha, Cinzinha e Cotoco.

Agradecimentos

Agradeço ao Dr. Eduardo Luiz Damiani Bica e ao Dr. Charles Bonatto por todo apoio e orientação que me deram ao longo deste trabalho.

Também agradeço às famílias Fattore e Serres, que me abrigaram sempre que precisei e cuja atenção jamais poderei retribuir à altura.

Não esquecerei jamais o apoio de Luciano Alexandre Pecetti e sua família.

Todos os colegas e amigos do Instituto de Física, em especial do Departamento de Astronomia, merecem meus mais sinceros agradecimentos.

Aos amigos da Hora Feliz, ao Renato Blumberg de Oliveira e ao Eduardo Balbinot, meus agradecimentos pela companhia, pelo chá e pela fogueira.

Resumo

Neste trabalho investigamos um dos processos que pode levar à formação de aglomerados abertos, focando-nos nas interações ocorridas durante a passagem de um aglomerado globular através do disco Galáctico, cujos efeitos podem resultar no surgimentos daqueles.

Tais interações podem ser uma alternativa aos cenários convencionais de formação estelar. Há diversos trabalhos explorando os efeitos, em nossa Galáxia, de impactos de nuvens HI, explosões de supernovas, galáxias canibalizadas ou aglomerados globulares, estes podendo inclusive ser núcleos de galáxias anãs capturadas pela Via Láctea, como parece ser o caso de ω Centauri. Trabalhos sobre interações de aglomerados globulares com o disco Galáctico invariavelmente tratam dos efeitos da Galáxia sobre o aglomerado globular, mas pouco tem sido feito com relação à análise de como os impactos de aglomerados globulares podem gerar o nascimento de aglomerados no disco Galáctico.

O presente trabalho investiga o caso envolvendo o aglomerado globular ω Centauri como projétil e os aglomerados abertos massivos BDSB 122 e Stephenson 2 como alvos resultantes do impacto de ω Centauri no disco Galáctico. ω Centauri é bem estudado na literatura, além de ser um dos mais massivos aglomerados globulares, tornando-o uma excelente escolha. A partir de seus dados de posição e movimento próprio fizemos diversas simulações numéricas com o método matemático *leap frog* implementado num código em linguagem C, o qual contém potenciais que representam a Galáxia com as componentes bojo, disco e halo. No caso particular dos aglomerados abertos, estimamos suas velocidades em torno do centro Galáctico pela curva de rotação da Via Láctea e consideramos que não possuem componente de velocidade perpendicular ao plano Galáctico.

A partir das simulações realizadas e das considerações sobre a perturbação causada por ω Centauri no disco Galáctico, mostramos a coincidência espacial e temporal existente entre os aglomerados envolvidos.

Abstract

In this work we investigate one of the processes that can lead to open cluster formation, focusing our analysis on the interactions occurring during a globular cluster crossing through Galactic disc.

These interactions can be an alternative to conventional scenarios of star formation. There are a number of papers exploring effects, in our Galaxy, such as HI cloud infall, supernovas explosions, cannibalized galaxies or globular clusters. The latter can be dwarf galaxy nuclei captured by the Milky Way. In particular this appears to be the case of ω Centauri. In general those works focus on the effects of the Galaxy on the globular cluster, but few deal with the effects of the impacts on generating cluster formation.

The present work investigates the case involving the globular cluster ω Centauri as a projectile and the open clusters BDSB 122 and Stephenson 2 as targets resulting from the impact of ω Centauri on the Galactic disk. ω Centauri is well studied, also being one of the most massive globular clusters, making it a good choice. From its position and proper motion data we made several numerical simulations using the leap frog method, implemented in a program on C language, which has potentials that describe the Galaxy with the bulge, disk and halo components. For the latter we estimated their velocities around Galactic center using the rotation curve, and assuming no velocity perpendicularly to the Galactic disk.

From our simulations and assumptions about perturbations generated by ω Centauri crossing the disc, we demonstrated the spatial and temporal coincidences between the studied clusters.

Sumário

| | |
|---|-----|
| Agradecimentos | ii |
| Sumário | v |
| Lista de Tabelas | vi |
| Lista de Figuras | vii |
| 1 Introdução | 1 |
| 2 On the possible generation of the young massive open clusters Stephen- son 2 and BDSB 122 by ω Centauri | 8 |
| 3 Conclusão e Perspectivas | 14 |
| 3.1 Importância do trabalho | 15 |
| 3.2 Perspectivas e Atualizações | 15 |
| Apêndice A A fossil bulge globular cluster revealed by VLT multi- conjugate adaptative optics | 18 |
| Referências Bibliográficas | 28 |

Lista de Tabelas

3.1 Novos aglomerados abertos na região do par estudado em nosso trabalho. 16

Lista de Figuras

| | | |
|-----|--|----|
| 1.1 | Exemplo de aglomerado globular, ω Centauri | 3 |
| 1.2 | Exemplo de aglomerado aberto, Stephenson 2 | 4 |
| 1.3 | Galáxia NGC 4559 | 5 |
| 1.4 | Galáxia Roda de Carroça | 6 |
| 1.5 | Figura de Vande Putte & Cropper (2009) mostrando o caso de NGC 6397 e NGC 6231. | 7 |
| 3.1 | Novos aglomerados no plano Galáctico | 17 |

Capítulo 1

Introdução

Dentre as diversas classes de objetos celestes, que servem de alvo e laboratório das pesquisas que buscam esclarecer nossa compreensão do Universo, os aglomerados estelares são uma escolha frequente. Através deles é possível o estudo da estrutura de braços espirais da Via Láctea ou sua curva de rotação, por exemplo. Outro tipo de informação que se pode obter a partir do estudo de aglomerados diz respeito aos mecanismos de formação estelar em sua história recente, no caso dos aglomerados abertos (Friel, 1995), que é um dos pontos de interesse abordados neste trabalho.

Historicamente os aglomerados Galácticos podem ser divididos em duas categorias distintas: os aglomerados abertos e os aglomerados globulares. A diferença mais evidente e comumente mencionada entre estas duas categorias de aglomerados diz respeito à aparente distribuição espacial das estrelas em seu interior. Os aglomerados globulares apresentam-se como uma distribuição estelar que visualmente sugere uma forma esférica. Diferentemente, os aglomerados abertos em geral não possuem distribuição espacial preferencial evidente de suas estrelas, aparecendo-nos como distribuições quase aleatórias, que leva-os a serem chamados de *abertos*. Uma outra característica marcante que difere estas duas categorias de aglomerados é a idade, já que os aglomerados globulares têm idades geralmente maiores do que uma dezena de bilhões de anos, enquanto parte relativamente pequena dos aglomerados abertos possui idade que ultrapasse 1 bilhão de anos. Também as populações estelares desses aglomerados possuem diferenças, já que as estrelas mais jovens, azuis e brilhantes são principalmente encontradas nos aglomerados abertos, enquanto as mais velhas e vermelhas nos aglomerados globulares. A massa é outro fator de separação desses grupos, já que apenas os poucos aglomerados abertos mais massivos, como

Westerlund 1 que tem massa da ordem de $10^5 M_{\odot}$ (Piatti et al., 1998, Clark et al., 2005), chegam a ter massas que se assemelham às massas típicas dos aglomerados globulares. A distribuição espacial dos aglomerados abertos situa-os em sua maioria como pertencentes ao disco Galáctico, o que no caso dos aglomerados globulares difere, visto situarem-se no bojo e halo da Via Láctea. Na Figura 1.1 é mostrado como exemplo de aglomerado globular um dos objetos estudados neste trabalho, ω Centauri. Na Figura 1.2, é apresentado Stephenson 2 como exemplo da categoria de aglomerados abertos. A partir de trabalhos como o de Hodapp (1994) surge uma outra categoria de aglomerados, os *embebidos*, que são assim chamados por ainda estarem imersos no material, basicamente gás e poeira, do qual suas estrelas nasceram (Lada & Lada, 2003).

O estudo pertinente aos mecanismos que disparam o nascimento de estrelas está em pauta desde os primórdios da Astrofísica. Há alguns processos classicamente associados à formação estelar, como por exemplo as ondas de densidade (Lin & Shu, 1964), os eventos de *supernovas* (Paczynski, 1998) e impactos no disco de nuvens de H I (Elmegreen et al., 2000), por exemplo. As ondas de densidade comprimem o material que encontram em seu deslocamento, disparando formação estelar e produzindo assim o padrão de braços que vemos em galáxias espirais. Nos eventos de supernovas, além de ser entregue material ao entorno da estrela que passa por essa fase evolutiva, a onda de choque gerada em sua explosão pode perturbar material que já exista na vizinhança e disparar a formação estelar. No intuito de abordar o caso da formação estelar a partir de um mecanismo alternativo, decidimos verificar a possibilidade da perturbação causada no disco Galáctico por colisões de aglomerados globulares induzir o nascimento de aglomerados abertos.

Durante a interação entre duas ou mais galáxias, são experimentadas forças que afetam suas estruturas e provocam choques, dos quais o efeito é a formação estelar (e.g. Hearn & Lamb, 2001). Entretanto, galáxias aparentemente isoladas também apresentam atividade de formação estelar, e parte dessa atividade pode ser associada às passagens dos aglomerados globulares pelo disco, como supomos. Muitos trabalhos têm sido publicados no sentido de investigar a passagem pelo disco dos aglomerados globulares Galácticos com foco no efeito que essas passagens causam sobre os próprios aglomerados globulares, como por exemplo os trabalhos de Dehnen et al. (2004) e Mastrobuono-Battisti et al. (2012). Entretanto a investigação dos efeitos da passagem dos aglomerados globulares sobre o meio interestelar é menos frequente (Wallin et al., 1996).

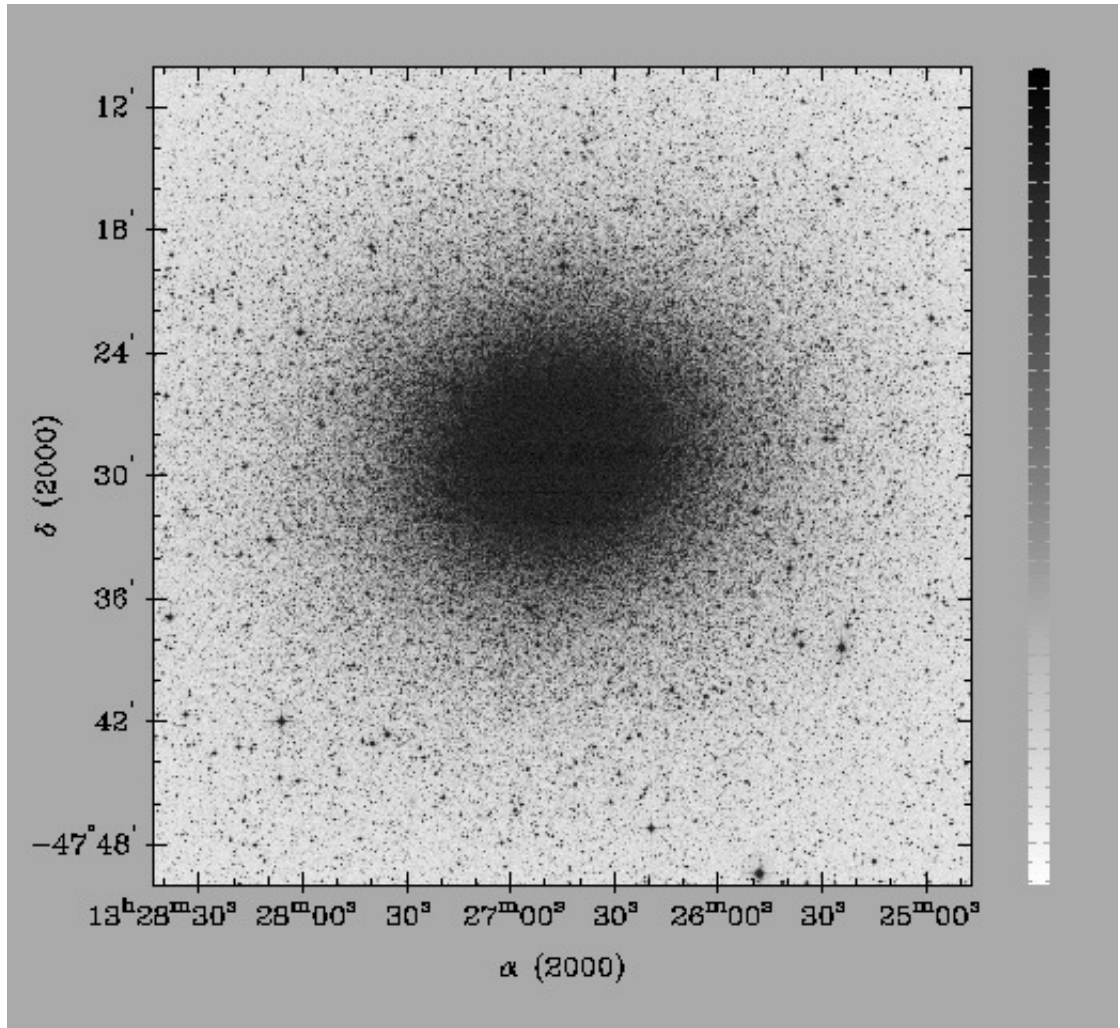


Figura 1.1: ω Centauri em Imagem na banda R do CADC^a.

^a<http://cadcwww.dao.nrc.ca/cadcbin/getdss>

Nesse cenário há casos de regiões de formação estelar em forma de anel, presentes em Galáxias como NGC 4559 que é uma espiral barrada, por exemplo. Na Figura 1.3 é destacada em tracejado branco a região abordada no artigo de Soria et al. (2004), em que há evidência destas formações. Estes anéis podem ser atribuídos à colisão de objetos relativamente massivos.

Um caso mais extremo e evidente é a galáxia Roda de Carroça (*Cartwheel*) (ESO 350-40), vista na Figura 1.4 (Higdon, 1995, Vorobyov, 2003), onde o peculiar anel externo é tido como resultante do impacto de uma galáxia anã.

O objetivo deste trabalho é realizar simulação da última passagem pelo disco da Via Láctea do aglomerado globular ω Centauri, buscando identificar relações entre

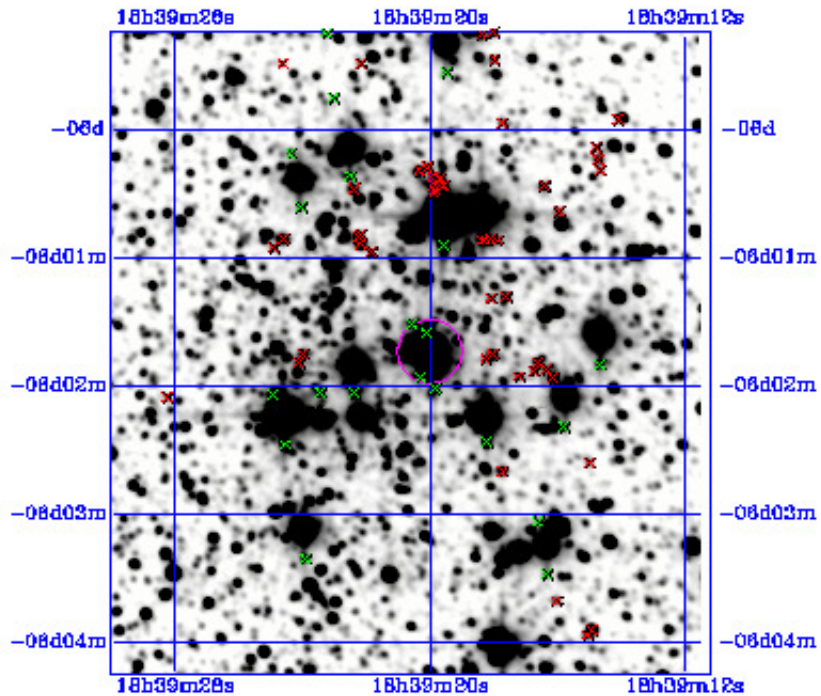


Figura 1.2: Aglomerado aberto, Stephenson 2. Imagem na banda K_s do 2MASS^a.

^a<http://www.ipac.caltech.edu/2mass/releases/allsky>

esse evento e a formação de aglomerados abertos, possivelmente resultantes deste impacto e propagação do choque.

Além do aglomerado globular ω Centauri no papel de projétil, foram selecionados os aglomerados abertos Stephenson 2 e BDSB 122 como candidatos a serem resultantes de seu impacto. No caso de ω Centauri esta seleção foi feita com base na disponibilidade de dados adequados para a simulação, além de ser massivo, o que o torna um excelente candidato a provocar perturbações em seu cruzamento pelo disco Galáctico. Já para os dois aglomerados abertos a seleção foi feita com base numa primeira estimativa de idade e posição, que poderiam associá-los ao instante da última passagem de ω Centauri pelo disco Galáctico.

Como apoio à nossa investigação encontramos na literatura o caso do par formado pelo aglomerado globular NGC 6397 e pelo aglomerado aberto NGC 6231. Tal caso foi abordado em Rees & Cudworth (2003) e Wright (2004), investigando a possível relação entre a passagem de NGC 6397 pelo disco Galáctico e o nascimento de NGC 6231. Para este par o trabalho de Vande Putte & Cropper (2009) mostrou que NGC 6231 não tem sua origem associada ao aglomerado globular NGC 6397, já

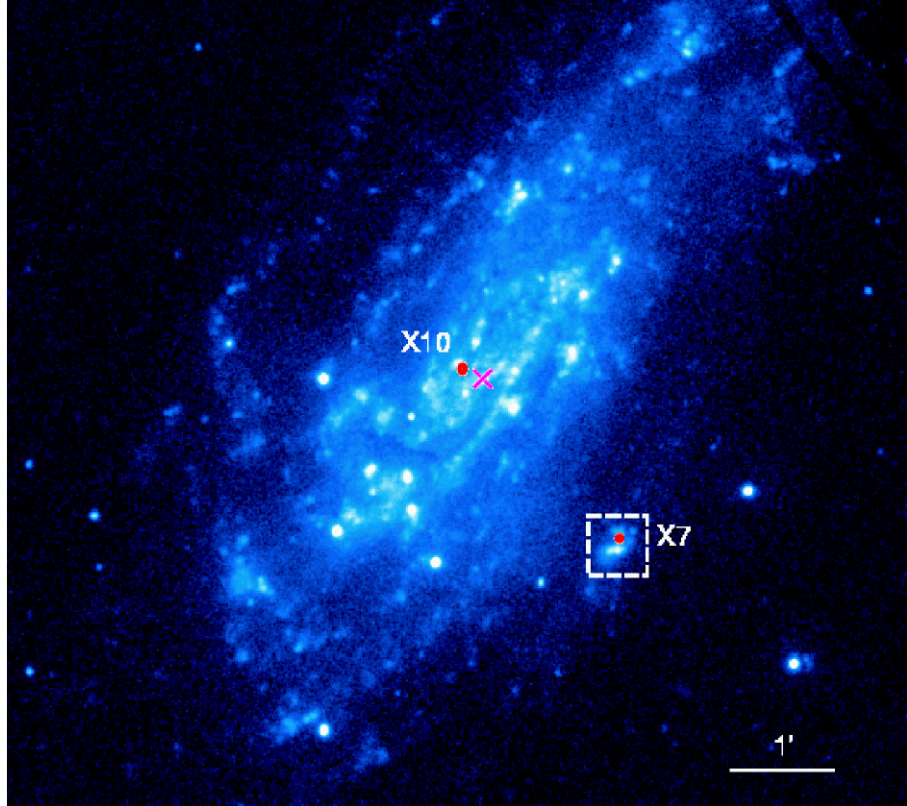


Figura 1.3: Imagem de NGC 4559 no ultravioleta, tirada com o *Optical Monitor* do XMM-Newton. A região tracejada mostra a área citada no artigo de Soria et al. (2004). O Norte fica para cima e o Leste para esquerda. Escala: $1'' \approx 45pc$.

que está tão distante do ponto de impacto de NGC 6397 que não há vínculos possíveis. Na Figura 1.5 é mostrada no plano Galáctico a posição de NGC 6231 e a região de impacto de NGC 6397 considerada em Vande Putte & Cropper (2009).

A seguir, no Capítulo 2, é apresentado o artigo no qual publicamos a análise de ω Centauri como possível gatilho da formação dos aglomerados abertos BDSB 122 e Stephenson 2 (Salerno et al., 2009).

No Capítulo 3 as conclusões do trabalho são apresentadas e perspectivas são levantadas.

No Apêndice A é apresentado um artigo para o qual realizamos a mesma abordagem de cálculo de órbitas do presente trabalho, mas aplicada ao aglomerado globular Galáctico HP 1, o qual localiza-se na porção central do bojo Galáctico. Essa posição de HP 1 apresentou desafios observacionais e testes para as teorias com respeito à sobrevivência de um aglomerado neste ambiente.

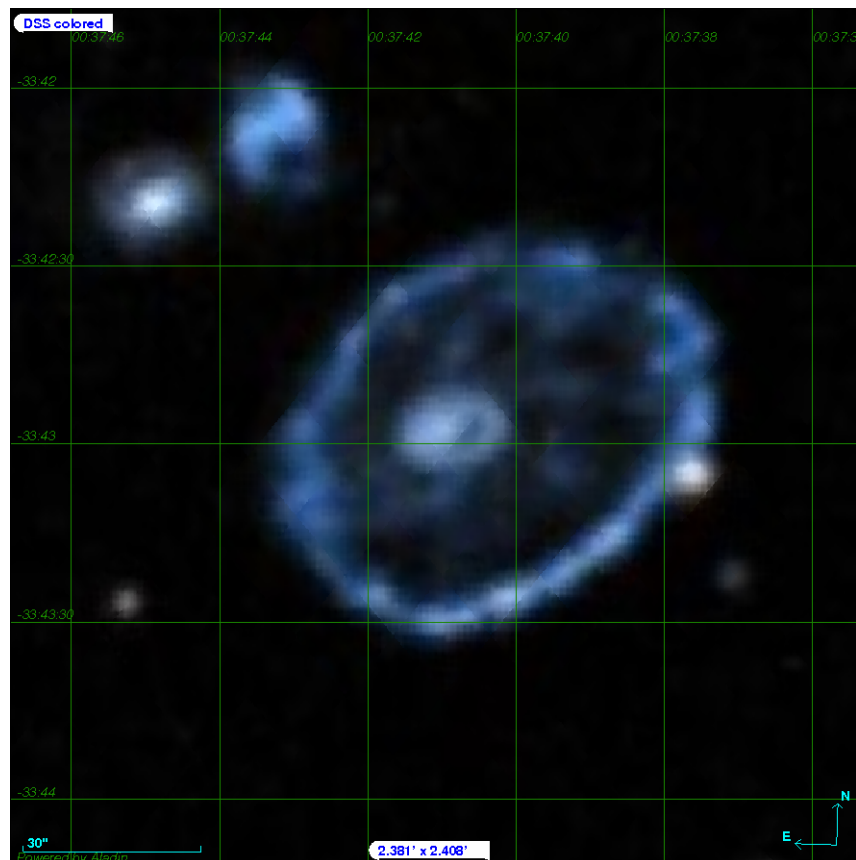


Figura 1.4: Galáxia Roda de Carroça (*Cartwheel Galaxy*) com seu anel peculiar. Imagem no óptico obtida do atlas *Aladin* (<http://aladin.u-strasbg.fr/java/nph-aladin.pl>) (Bonnarel et al., 2000).

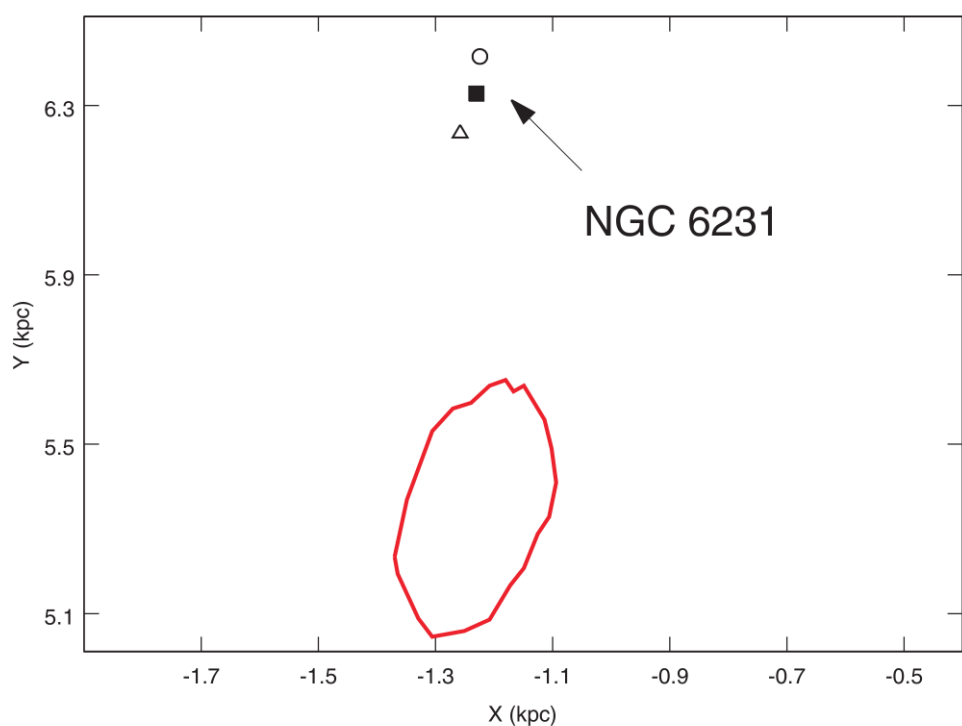


Figura 1.5: Figura de Vande Putte & Cropper (2009) que mostra em vermelho a região considerada para o impacto de NGC 6397. As posições média, mínima e máxima de NGC 6231 são assinaladas pelos símbolos pretos.

Capítulo 2

**On the possible generation of the
young massive open clusters
Stephenson 2 and BDSB 122 by
 ω Centauri**

On the possible generation of the young massive open clusters Stephenson 2 and BDSB 122 by ω Centauri

G. M. Salerno¹, E. Bica¹, C. Bonatto¹, and I. Rodrigues²

¹ Universidade Federal do Rio Grande do Sul, Departamento de Astronomia CP 15051, RS, Porto Alegre 91501-970, Brazil
 e-mail: [salerno; bica; charles]@if.ufrgs.br; irapuan@univap.br

² IP&D - Universidade do Vale do Paraíba - UNIVAP, Av. Shishima Hifumi, 2911 - Urbanova, São José dos Campos 12244-000, SP, Brazil

Received 27 January 2009 / Accepted 10 February 2009

ABSTRACT

Context. Passing through the disk of a galaxy, a massive object such as a globular cluster can trigger star formation.
Aims. We test the hypothesis that the most massive globular cluster in the Galaxy, ω Centauri, which crossed the disk approximately 24 ± 2 Myr ago, may have triggered the formation of the open clusters Stephenson 2 and BDSB 122.

Methods. The orbits of ω Centauri, Stephenson 2, and BDSB 122 are computed for the three-component model of Johnston, Hemquist & Bolte, which considers the disk, spheroidal, and halo gravitational potentials.

Results. With the reconstructed orbit of ω Centauri, we show that the latest impact site is consistent, within significant uncertainties, with the birth-site of the young massive open clusters BDSB 122 and Stephenson 2. Within the uncertainties, this scenario is consistent with the timescale of their backward motion in the disk, shock propagation and delayed star formation.

Conclusions. Together with open cluster formation associated with density waves in spiral arms, the present results are consistent with massive globular clusters being additional progenitors of open clusters, the most massive ones in particular.

Key words. galaxy: globular clusters: individual: ω Centauri – galaxy: open clusters and associations: individual: BDSB – Galaxy: open clusters and associations: individual: Stephenson 2

1. Introduction

Disk-stability criteria and impact assumptions suggest that the passage of a globular cluster (GC) can trigger a bubble or wave of self-propagating star formation within the disk of the Galaxy (Walla et al. 1996). The initial mechanical perturbation produces a local enhancement in the interstellar medium (ISM) density, from which localised star formation may occur. Subsequently, clustered star formation may happen along the border of a radially expanding density wave or ionisation front (e.g., Soria et al. 2005 – hereafter SCP05; Elmegreen & Lada 1977; Whitworth et al. 1994). The expanding bubble is capable of compressing the neutral ISM above the stability criterion against gravitational collapse. Alternative star-formation triggering mechanisms are the infall of a high-velocity HI cloud (Elmegreen et al. 2000; Larsen et al. 2002), or hypernova explosions (Paczynski 1998).

Prominent, isolated star-forming bubbles have been observed in external galaxies. A bubble of diameter ≈ 600 pc was detected in NGC 6946 (Larsen et al. 2002), containing a young super star cluster and at least 12 surrounding young clusters, the latter being comparable in luminosity to the most luminous Galactic OCs. The triggering mechanism in NGC 6946 appears to be the impact of a high-velocity HI cloud and/or hypernova explosions (Elmegreen et al. 2000). The Galaxy may harbour similar structures, a possible example being the Cygnus superbubble, which contains OB associations (Vlemmings et al. 2004, and references therein).

For a GC, the triggering effects are essentially gravitational. A natural assumption is that GCs, crossing the disk every 1 Myr on average, may be responsible for some star formation. A possible case relates the origin of the OC NGC 6231 to the

GC NGC 6397 disk-crossing (Rees & Cudworth 2003). Another possibility is that the low-mass GC FSR 584 has triggered star formation in the W 3 complex (Bica et al. 2007).

The OCs Stephenson 2 and BDSB 122 were discovered in 1990 (Stephenson 1990) and 2003 (Bica et al. 2003), respectively. 2MASS¹ images of both clusters are shown in Fig. 1. The suspected richness of Stephenson 2 in red supergiants was confirmed by Nakaya et al. (2001) and Ortolani et al. (2002), providing an age of ≈ 20 Myr, and a distance from the Sun of $d_{\odot} = 6$ kpc (Ortolani et al. 2002). Both clusters are among the most massive OCs known in the Galaxy. BDSB 122 has 14 red supergiants, is located at $d_{\odot} = 5.8$ kpc from the Sun, and has an estimated mass of $2-4 \times 10^4 M_{\odot}$, and an age of 7–12 Myr (Figer et al. 2006). Stephenson 2 has 26 red supergiants, is located at $d_{\odot} = 5.8^{+1.9}_{-0.8}$ kpc from the Sun, has an estimated mass of $4 \times 10^4 M_{\odot}$, and an age of 12–17 Myr (Davies et al. 2007). Their distances from the Sun are identical, within uncertainties, and their projected separation on the sky is ≈ 100 pc. The designation Stephenson 2 was originally assigned by Ortolani et al. (2002), and also adopted by Dias et al. (2002, and updates). Stephenson 2 and BDSB 122 are clearly in the red supergiant (RSG) phase (Bica et al. 1990). Davies et al. (2007) referred to these clusters as RSGC 1 and RSGC 2, respectively.

The positions (and uncertainties) of both clusters, together with ω Centauri (NGC 5139), are shown in Fig. 2 superimposed on a schematic view of the Milky Way (based on Momany et al. 2006; and Drimmel & Spergel 2001). BDSB 122 and Stephenson 2 are slightly closer to the Galactic centre than the Scutum-Crux arm. Several other young clusters from the

¹ <http://www.ipac.caltech.edu/2mass/releases/allsky>

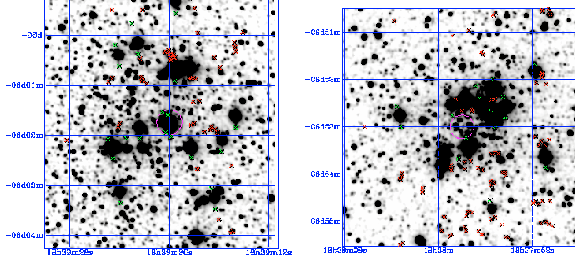


Fig. 1. $5' \times 5'$ 2MASS K_s images of Stephenson 2 (left) and BDSB 122 (right). Figure orientation: North to the top and East to the left.

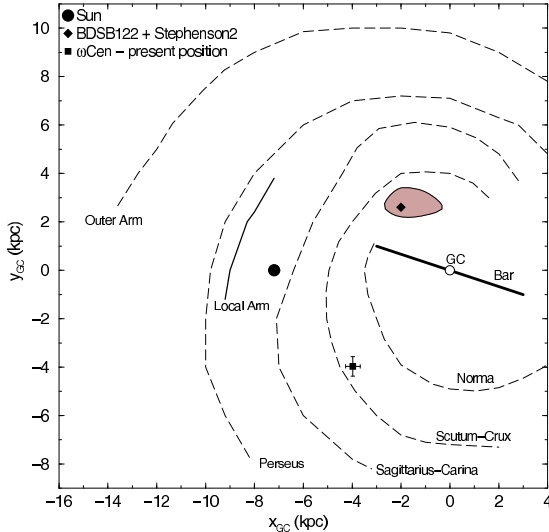


Fig. 2. The present-day positions (and uncertainties) of Stephenson 2, BDSB 122, and ω Centauri overplotted on a schematic projection of the Galaxy as seen from the North pole, with 7.2 kpc as the Sun's distance to the Galactic centre. Main structures are identified.

catalogues of [Bica et al. \(2003\)](#) and [Dutra et al. \(2003\)](#) have already been studied in detail (e.g., [Soares et al. 2008](#); [Ortolani et al. 2008](#); [Hanson & Bubnick 2008](#)).

We trace the orbits of both ω Centauri and Stephenson 2 backwards in time (and consequently, also that of BDSB 122) in the disk, testing an impact hypothesis for the origin of these two massive OCs. Using as constraints the GC space velocity, orbit integrations in the Galactic potential have been applied widely to 54 GCs (e.g., [Dinescu et al. 2003](#); [Allen et al. 2008](#)).

This paper is structured as follows. In Sect. 2 we study the past orbit of ω Centauri. In Sect. 2.1, the past orbits of Stephenson 2 and ω Centauri are compared to search for spatial and time coincidence. Our conclusions are presented in Sect. 3.

2. ω Centauri as a projectile

The most massive Galactic GC, ω Centauri ($4 \times 10^6 M_\odot$ – [Nakaya et al. 2001](#)), has a metallicity spread and a flat density distribution typical of a dwarf galaxy nucleus captured by the Galaxy ([Bekki & Freeman 2003](#)). Thus, irrespective of the existence of young massive clusters, in some way associated with the impact site, the orbit of ω Centauri in the Galactic potential

Table 1. Present-day cluster positions.

| Cluster | ℓ ($^\circ$) (1) | b ($^\circ$) (2) | $\alpha(J2000)$ (h:m:s) (3) | $\delta(J2000)$ ($^\circ$, ' $''$) (4) | | (5) |
|-------------------|-------------------------------|----------------------------|-----------------------------------|---|--|-----|
| ω Centauri | 309.10 | +14.97 | 13:26:46 | -47:28:37 | | |
| BDSB 122 | 26.84 | +0.65 | 18:37:58 | -6:53:00 | | |
| Stephenson 2 | 26.18 | -0.06 | 18:39:20 | -6:01:44 | | |

is worth consideration in searching, in particular, for the effects of the last disk passage. Evidence of a similar disk impact and a star-forming event has been observed in the spiral galaxy NGC 4559 with Hubble Space Telescope (HST), XMM-Newton, and ground-based (SCP05) data. The age of the star-forming complex, which has a ring-like distribution, is $\lesssim 30$ Myr. It appears to be an expanding wave of star formation, triggered by an initial density perturbation. The most likely triggering mechanism was a collision with a satellite dwarf galaxy crossing through the gas-rich outer disk of NGC 4559, which may have been the dwarf galaxy visible a few arcsec to the NW of the complex. This scenario is reminiscent of a scaled-down version of the Cartwheel galaxy ([Struck-Marcell & Higdon 1993](#); [Struck-Marcell et al. 1996](#)).

As another example, proper motions (PMs) and radial velocity suggest that the GC NGC 6397 crossed the Galactic disk 5 Myr ago, possibly triggering the formation of the OC NGC 6231 ([Rees & Cudworth 2003](#)), and thus lending support to the present scenario ([Wallin et al. 1996](#)). NGC 6397 and NGC 6231 are closely projected on the sky ($\Delta\ell \approx 5^\circ$, $\Delta b \approx 13^\circ$). However, in the case of the disk-crossing of ω Centauri being the possible triggering mechanism of BDSB 122 and Stephenson 2, the GC is now widely apart from the pair of massive OCs ($\Delta\ell \approx 77^\circ$, $\Delta b \approx 15^\circ$). Thus, PM and radial velocity are fundamental constraints for the analysis of ω Centauri, and impact solutions require a detailed integration of its orbit across the Galactic potential.

2.1. Orbit computation

We employ a three-component mass-distribution model of the Galaxy resembling that in the study of a high-velocity black hole on a Galactic-halo orbit in the solar neighbourhood ([Mirabel et al. 2001](#), and references therein). In short, we use the three-component model of [Johnston et al. \(1996\)](#) – hereafter JHB96 – in which the disk, spheroidal, and halo gravitational potentials are described by $\phi_{\text{disk}}(R, z) = -GM_{\text{disk}}/\sqrt{R^2 + (a + \sqrt{z^2 + b^2})^2}$ ([Miyamoto & Nagai 1975](#)), $\phi_{\text{spher}}(R) = -\frac{GM_{\text{spher}}}{R+c}$ ([Hernquist 1990](#)), and $\phi_{\text{halo}}(R) = v_{\text{halo}}^2 \ln(R^2 + d^2)$, where $M_{\text{disk}} = 1 \times 10^{11} M_\odot$, $M_{\text{spher}} = 3.4 \times 10^{10} M_\odot$, $v_{\text{halo}} = 128 \text{ km s}^{-1}$, R and z are the cylindrical coordinates, and the scale lengths $a = 6.5 \text{ kpc}$, $b = 0.26 \text{ kpc}$, $c = 0.7 \text{ kpc}$, and $d = 12.0 \text{ kpc}$. Table 1 shows the Galactic and Equatorial coordinates of the three clusters. Following [Mizutani et al. \(2003\)](#), the relevant parameters for computing the motion of ω Centauri are the distance from the Sun $d_\odot = 5.3 \pm 0.5 \text{ kpc}$, the PM components (mas yr^{-1}) $\mu_\alpha \cos(\delta) = -5.08 \pm 0.35$ and $\mu_\delta = -3.57 \pm 0.34$, and finally the heliocentric radial velocity $V_r = 232.5 \pm 0.7 \text{ km s}^{-1}$.

The models were computed with $R_{\text{GC}} = 7.2 \text{ kpc}$ ([Bica et al. 2006](#)) as the distance of the Sun to the Galactic centre. The Galactic velocities of ω Centauri are $U = 54.3 \pm 9.5 \text{ km s}^{-1}$,

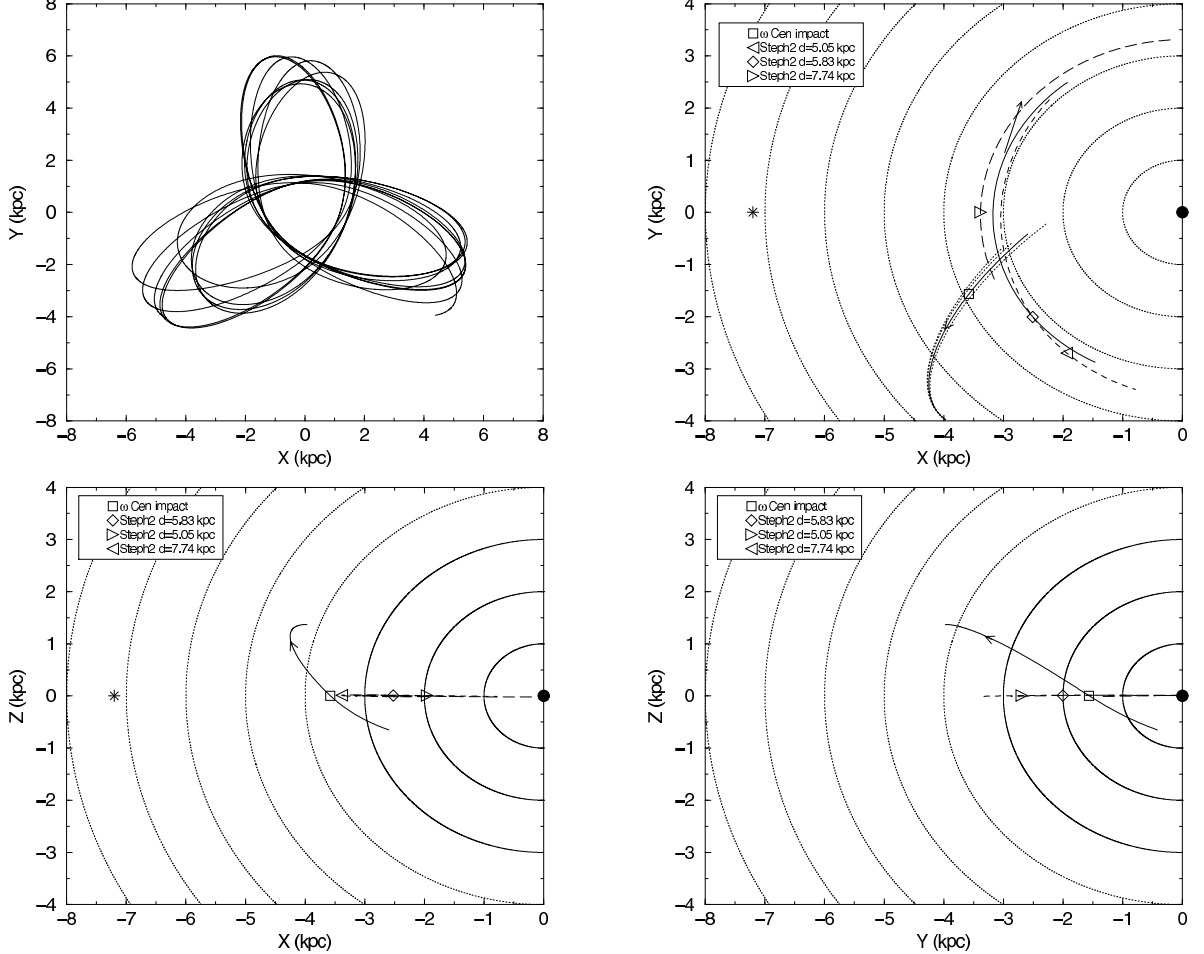


Fig. 3. Top-left panel: galactocentric XY-plane projection of the ω Centauri orbit over the past 2 Gyr. Top-right: the past 30 Myr orbit of ω Centauri (solid line) for $R_{GC} = 7.2$ kpc. Additional neighbouring orbits (dotted) are, from bottom to top: JHB96 (-10%), JHB96 ($+10\%$), FSC96. The impact site on the disk is shown by the empty square. Arrows indicate orbit direction. Orbits of Stephenson 2 for the assumed distance from the Sun (and uncertainties) are shown. The corresponding XZ and YZ projections are in the bottom panels. Empty symbols over the Stephenson 2 orbits indicate its possible positions 24 Myr ago. The Sun at its present position (asterisk) and the Galactic Centre (filled circle) are shown.

$V = -44.2 \pm 8.2 \text{ km s}^{-1}$, and $W = -1.3 \pm 13.0 \text{ km s}^{-1}$. Alternatively, we also computed orbits with $R_{GC} = 7.6$ kpc, which was the value obtained by Eisenhauer et al. (2005). By means of the statistical parallax of central stars, it should be noted that Trippe et al. (2008) found $R_{GC} = 8.07 \pm 0.32$ kpc, while Ghez et al. (2008), with the orbit of one star close to the black hole, found $R_{GC} = 8.0 \pm 0.6$ kpc or $R_{GC} = 8.4 \pm 0.4$ kpc, under different assumptions. Cluster distances are heliocentric, and therefore do not depend on R_{GC} ; on the other hand, the value of R_{GC} has some effect on the potentials, and can thus, affect the orbit computation. Since the difference between the adopted value of R_{GC} and the more recent measurements is insignificant, the value of R_{GC} should not influence significantly the present results.

Based on the rotation curves of Brand & Blitz (1993) and Russeil (2003), and an estimate with the galaxy mass model described above (Mirabel et al. 2001), we derived the orbital velocity of Stephenson 2 to be $V_c = 214 \pm 4 \text{ km s}^{-1}$. The nearly

flat Galactic rotation curve at the Stephenson 2 position allows us to adopt this circular velocity also for the orbits corresponding to distance uncertainties (Sect. 1). The orbit of ω Centauri, computed back over 2 Gyr, is comparable to that derived by Mizutani et al. (2003), in particular its Rosette pattern, which is projected on the XY plane (Fig. 3). The simulation indicates that ω Centauri collided with the disk as recently as 24 ± 2 Myr ago. This is so short a time that fossil remains of this event may nowadays be detectable in the disk.

Figure 3 (top-left panel) shows the Galactic XY-plane projection of the orbital motion of ω Centauri during the past 2 Gyr. In the remaining panels, we focus on the past 30 Myr of the motion of ω Centauri and Stephenson 2. For Stephenson 2, we consider the different orbits resulting from the adopted distance from the Sun and their corresponding uncertainties (Sect. 1). It is interesting that the orbit of Stephenson 2 passes close to the impact site of ω Centauri at a comparable time, within the uncertainties (see below). Since Stephenson 2 and

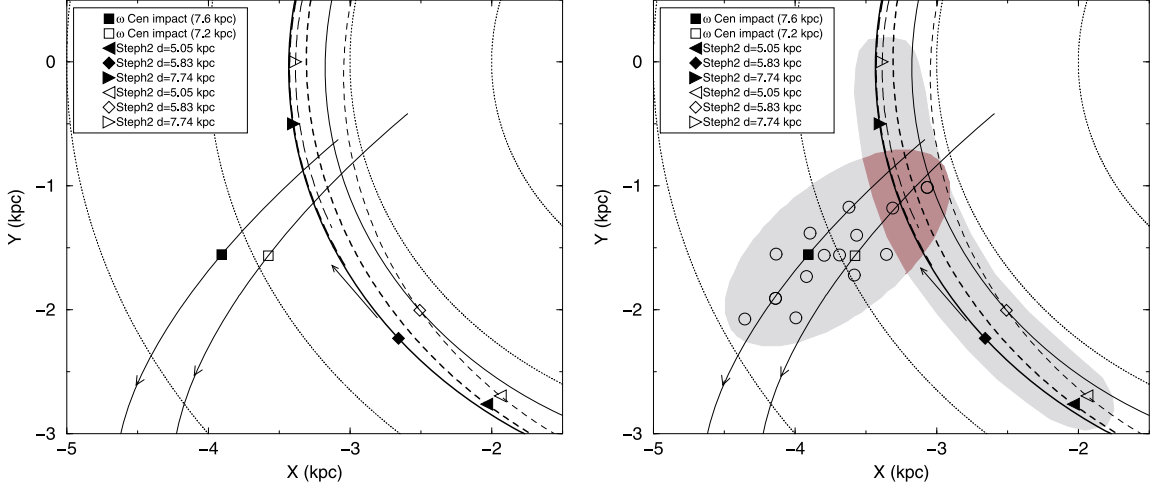


Fig. 4. Close-up of the impact site. *Left panel:* orbits computed with $R_{\text{GC}} = 7.2 \text{ kpc}$ (empty symbols) and $R_{\text{GC}} = 7.6 \text{ kpc}$ (filled symbols). *Right:* same as left panel but including error distribution for the ω Centauri impact site and Stephenson 2 proto-cluster position. A random selection of impact sites (open circles) is shown within the ω Centauri error ellipsoid.

BDSB 122 have almost the same position (within the uncertainties), the same conclusions hold for the latter cluster. The XZ and YZ-plane projections (bottom panels) indicate that ω Centauri emerged at $\approx 45^\circ$ from the plane to its present position.

To probe orbital uncertainties owing to the adopted potential, we also employed the potential model of Flynn et al. (1996) – hereafter FSC96 – and tested consequences of variations of $\pm 10\%$ in the input parameters of JHB96. The results are shown in Fig. 3 (top-right panel), from which we conclude that orbit variations due to the adopted potential are much smaller than our error ellipsoid (Fig. 4, right panel).

Close-ups of the ω Centauri impact site and the back-traced positions of Stephenson 2 are shown in Fig. 4 (left panel) for a Sun's distance from the Galactic centre of both 7.2 kpc and 7.6 kpc. It is clear that the value of 7.6 kpc does not significantly alter the orbit of the encounter. The right panel shows the error ellipsoid of several impact site simulations computed by varying initial conditions according to the errors in the different relevant input quantities. The ellipsoid reflects variations implied by velocity uncertainties in the PM, radial velocity and present position of ω Centauri along the line of sight in the (U, V, W) velocities. The impact obtained with a Galactocentric distance $R_{\text{GC}} = 7.6 \text{ kpc}$ is also shown. The disk-orbit of Stephenson 2 crosses the ω Centauri ellipsoid error distribution. The range in impact site to proto-cluster separations contains distances smaller than $\approx 1 \text{ kpc}$, with an average separation of $\sim 500 \text{ pc}$ (intersection area in Fig. 4, right panel). Larger separations would require prohibitive expansion velocities, despite the fact that we are dealing with an encounter in a denser, central part of the disk, while in NGC 4559, the event was external.

For the GC-induced formation hypothesis to be valid, the timescales associated with the onset of star formation (after impact), duration of star formation and the cluster age, should be compatible with the disk-crossing age. Following Vande Putte & Cropper (2009), the first timescale is not well known, ranging from virtually instantaneous, i.e. negligible compared to the cluster age, to 15 Myr (Lépine & Duvert 1994) and 30 Myr (Wallin et al. 1996). The star formation timescale may be short,

$\approx 2 \times 10^5 \text{ yr}$, as suggested by McKee & Tan (2002) for stars more massive than $8 M_\odot$. Given that the ages of Stephenson 2 and BDSB 122 are within the ranges of 12–17 Myr and 7–12 Myr, respectively, ω Centauri, which crossed the disk $\approx 24 \text{ Myr}$ ago, may have triggered their formation only if the star formation started during a time period of less than $\approx 15 \text{ Myr}$, which is within the accepted range. In the case of NGC 4559, these combined timescales are less than $\sim 30 \text{ Myr}$ (Soria et al. 2005).

The above clues suggest that the most recent crossing of ω Centauri through the disk occurred close to the sites where two massive OCs were formed. Both Stephenson 2 and BDSB 122 are younger than the age of the impact, and the differences in age of a few Myr are consistent with the shock propagation and subsequent star formation. The overall evidence gathered in the present analysis supports ω Centauri being the origin of this localised star formation in the Galaxy, which harbours two of the more massive known OCs.

This work suggests a scenario where the disk passage of GCs can generate OCs, massive ones in particular, as indicated by the orbit of ω Centauri and its impact site. As a consequence, OC formation is not induced entirely by the spiral density wave mechanism in spiral arms.

3. Summary and conclusions

Globular clusters orbiting the bulge and halo of the Galaxy cross the disk on average once every 1 Myr, and these events are expected to produce significant physical effects on the disk. For instance, the impact of a GC passing through the disk can trigger star formation either by the accumulation of gas clouds around the impact site or by the production of an expanding mechanical wave. Time delays are expected in both cases because of the collapse and fragmentation of molecular clouds before star formation. This phenomenon was observed in the galaxy NGC 4559 (e.g., SCP05). If this mechanism operates frequently in the Galaxy, the most massive GC ω Centauri can be assumed to be an ideal projectile for analysing the state of its last impact site in the disk.

Since ω Centauri collided with the Galactic disk \approx 24 Myr ago, a major star-forming event appears to have occurred close (\lesssim 1 kpc) to the impact locus that generated two of the most massive young OCs known in the Galaxy, BDSB 122 and Stephenson 2. We suggest a connection between these events that is similar to that between the impact and shock observed in NGC 4559 (SCP05). We use a model of the Galactic potential to integrate the orbit of ω Centauri. As shown in Fig. 4, when the uncertainties in space velocity, distances, and potential are considered, the error distributions of the ω Centauri impact site and the birth-site of Stephenson 2 overlap. This overlap suggests a scenario where the disk passage and formation of the pair of OCs may be physically connected. Alternatively, the time coincidence may have occurred within a separation \lesssim 1 kpc. In such a case, the expanding bubble scenario such as that in NGC 4559 would apply. The latter case is more probable, since two clusters have been formed.

Levy (2000) performed 2D hydrodynamic simulations to study the impact of GCs on the Galactic disk in the presence of available gas. They found that the moving GC causes a shock in the gas that propagates through the disk on a kpc scale, thus producing star formation. Vande Putte & Cropper (2009) simulated in detail the effects of GC impacts on the disk, basically confirming the results of Wallin et al. (1996) and Levy (2000), even in the absence of gas at the impact site. They found a concentration of disk material compressed to a scale of \sim 10 pc, which may subsequently attract gas leading to star formation. The compression increases with the GC mass.

At this point, an interesting question arises. For a rate of \sim 1 GC impact per Myr, a high probability is expected of one GC impact occurring within 1–2 kpc of any location within the inner Galaxy in about 10 Myr. However, the star-formation efficiency of these events appears to be low, according to Vande Putte & Cropper (2009), who found that of the 54 GCs with accurate proper motions studied by them, only three appear to be associated with young OCs. It is possible that conditions such as GC mass and impact site properties, and the availability of molecular gas, temperature and density, constrain the star-formation efficiency.

Evidence drawn from the present work suggests that GCs can be progenitors of massive OCs. We have focused in particular on ω Centauri. Density-wave shocks may not be the only cause of the formation of the more massive OCs, which is a possibility to be further explored, both theoretically and observationally.

Acknowledgements. We thank the anonymous referee for suggestions. We acknowledge partial support from CNPq (Brazil).

References

- Allen, C., Moreno, E., & Pichardo, B. 2008, ApJ, 674, 237
- Bekki, K., & Freeman, K.C. 2003, MNRAS, 346, L11
- Bica, E., Santos, Jr., J. F. C., & Alloin, D. 1990, A&A, 235, 103
- Bica, E., Dutra, C. M., Soares, J., & Barbuy, B. 2003, A&A, 400, 533
- Bica, E., Bonatto, C., Barbuy, B., & Ortolani, S. 2006, A&A, 450, 105
- Bica, E., Bonatto, C., Ortolani, S., & Barbuy, B. 2007, A&A, 472, 483
- Brand, J., & Blitz, L. 1993, A&A, 275, 67
- Davies, B., Figer, D. F., Kudritzki, R.-P., et al. 2007, ApJ, 671, 781
- Dias, W. S., Alessi, B. S., Moitinho, A., & Lépine, J. R. D. 2002, A&A, 389, 871
- Dinescu, D. I., Girard, T. M., van Altena, W. F., & López, C. E. 2003, AJ, 125, 1373
- Drimmel, R., & Spergel, D. N. 2001, ApJ, 556, 181
- Dutra, C. M., Bica, E., Soares, J., & Barbuy, B. 2003, A&A, 404, 223
- Eisenhauer, F., Genzel, R., Alexander, T., et al. 2005, ApJ, 628, 246
- Elmegreen, B. G., & Lada, C. J. 1977, ApJ, 214, 725
- Elmegreen, B. G., Efremov, Y. N., & Larsen, S. 2000, ApJ, 535, 748
- Figer, D. F., MacKey, J. W., Robberto, M., et al. 2006, ApJ, 643, 1166
- Flynn, C., Sommer-Larsen, J., & Christensen, P. R. 1996, MNRAS, 281, 1027
- Ghez, A. M., Salim, S., Weinberg, N. N., et al. 2008, ApJ, 689, 1044
- Hanson, M. M., & Bubnick, B. F. 2008, PASP, 120, 150
- Hernquist, L. 1990, ApJ, 356, 359
- Johnston, K. V., Hernquist, L., & Bolte, M. 1996, ApJ, 465, 278
- Larsen, S. S., Efremov, Y. N., Elmegreen, B. G., et al. 2002, ApJ, 567, 896
- Lépine, J. R. D., & Duvert, G. 1994, A&A, 286, 60
- Levy, V. V. 2000, A&AT, 18, 621
- McKee, C. F., & Tan, J. C. 2002, Nature, 416, 59
- Mirabel, I. F., Dhawan, V., Mignani, R. P., & Rodrigues, I. 2001, Nature, 413, 139
- Miyamoto, M., & Nagai, R. 1975, PASJ, 27, 533
- Mizutani, A., Chiba, M., & Sakamoto, T. 2003, ApJ, 589, L89
- Momany, Y., Zaggia, S., Gilmore, G., et al. 2006, A&A, 451, 515
- Nakaya, H., Watanabe, M., Ando, M., Nagata, T., & Sato, S. A. 2001, AJ, 122, 876
- Paczyński, B. 1998, ApJ, 494, L45
- Rees, R. F., & Cudworth, K. M. 2003, BAAS, 35, 1219
- Russeil, D. 2003, A&A, 397, 133
- Soares, J., Bica, E., Ahumada, A. V., & Clariá, J. J. 2008, A&A, 478, 419
- Soria, R., Cropper, M., & Pakull, M. 2004, RMxAC, 20, 57
- Soria, R., Cropper, M., Pakull, M., Mushotzky, R., & Wu, K. 2005, MNRAS, 356, 12
- Stephenson, C. B. 1990, AJ, 99, 1867
- Struck-Marcell, C., & Higdon, J. L. 1993, ApJ, 411, 108
- Struck-Marcell, C., Appleton, P. N., Bome, K. D., & Lucas, R. A. 1996, AJ, 112, 1868
- Trippe, S., Gillessen, S., Gerhard, O. E., et al. 2008, A&A, 492, 419
- Vande Putte, D., & Cropper, M. 2009, MNRAS, 392, 113
- Vlemmings, W. H. T., Cordes, J. M., & Chatterjee, S. 2004, ApJ, 610, 402
- Wallin, J. F., Higdon, J. L., & Staveley-Smith, L. 1996, AJ, 459, 555
- Whitworth, A. P., Bhattacharjee, A. S., Chapman, S. J., Disney, M. J., & Turner, J. A. 1994, A&A, 290, 421

Capítulo 3

Conclusão e Perspectivas

Foi apresentado um estudo da órbita do aglomerado globular ω Centauri e dos aglomerados abertos massivos Stephenson 2 e BDSB 122. Para esse fim calculamos, através de uma rotina do programa *IDL*[®], as posições X, Y e Z bem como as velocidades iniciais U, V e W dos objetos, num referencial com origem no centro Galáctico, eixo X apontando do Sol para o centro da Via Láctea, eixo Y no sentido de rotação da Galáxia e eixo Z na direção do norte Galáctico. Com estas informações o programa de simulação, que usa o método *leap frog*, calculou a posição de nossos objetos em direção ao passado de suas órbitas, dentro de um potencial com as componentes descritas no Capítulo 2. Esse programa foi escrito por Irapuan Rodrigues para sua colaboração em Mirabel et al. (2001). A partir das informações orbitais obtidas construímos gráficos que foram usados no intuito de estabelecer vínculos de idade e posição, testando a hipótese de conexão entre a passagem de ω Centauri pelo disco Galáctico e a formação dos aglomerados abertos massivos Stephenson 2 e BDSB 122.

Nesse processo pudemos concluir que a colisão gravitacional de objetos massivos no disco Galáctico, tais como os aglomerados globulares, podem ser mais um mecanismo significativo de disparo da formação de aglomerados abertos.

Participamos com o mesmo tipo de abordagem deste trabalho em Ortolani et al. (2011), que pode ser visto no Apêndice A. Nossa contribuição, no sentido de fortalecer as conclusões ali presentes, foi simular a órbita do aglomerado globular HP 1, da mesma forma que procedemos para o caso de ω Centauri, verificando-se que HP 1 é pertencente ao bojo Galáctico.

3.1 Importância do trabalho

A importância deste trabalho reside na contribuição à investigação de um mecanismo adicional de como se dão os nascimentos dos aglomerados abertos, juntando-se aos demais processos comumente abordados na literatura. Existem poucos trabalhos publicados com o enfoque que aqui adotamos, sendo exemplos os artigos de Rees & Cudworth (2003) e Wright (2004). Logo, é fundamental que se aborde esta classe de problemas com mais profundidade e abrangência, visando formar um conjunto consistente de informações teóricas, observacionais e computacionais, para que se possa vincular com mais robustez as colisões gravitacionais de aglomerados globulares com a formação de uma fração dos aglomerados abertos do disco Galáctico. Ressaltando-se que, no caso particular de ω Centauri, nossa investigação evidenciou, dentro das incertezas, seu vínculo com a formação dos aglomerados massivos do disco Galáctico Stephenson 2 e BDSB 122.

3.2 Perspectivas e Atualizações

Uma das perspectivas deste trabalho é a extensão do estudo para uma lista maior de aglomerados globulares, cujos integrantes, baseados em suas massas e órbitas, tenham maiores chances de serem protagonistas de eventos de formação estelar, particularmente de aglomerados abertos no disco Galáctico. Com esse novo conjunto de simulações poderemos ter uma visão geral dos processos envolvidos, assim como da dimensão da participação desse fenômeno na função de gatilhos de formação estelar.

Com os refinamentos em observações e métodos, como por exemplo em Ortolani et al. (2011) e no catálogo UCAC4 (Zacharias et al., 2013), o futuro desta linha de trabalho será promissor, visto que uma de nossas limitações é a precisão das medidas de movimento próprio. Nesse cenário barras de erro menores levam a vínculos mais sólidos na região de interação entre aglomerados abertos e aglomerados globulares aumentando a confiabilidade dos resultados.

Os avanços na determinação dos parâmetros dinâmicos dos aglomerados, também abrem a possibilidade de estender as análises até a penúltima passagem dos aglomerados globulares pelo disco Galáctico. O aumento de casos de estudo

formará uma amostra ainda mais significativa de eventos para fortalecer investigações como a presente.

Somando-se a isso, a descoberta de novos aglomerados abertos incrementa a lista de possíveis objetos relacionados ao evento que abordamos. Na Tabela 3.1 mostramos 4 novos aglomerados abertos descobertos na região do par Stephenson 2/BDSB 122, após a finalização do artigo.

| Aglomerado | l (graus) | b (graus) | Distância (Kpc) | Idade (M_{anos}) | Referência |
|-------------------|----------------|----------------|--------------------|-------------------------|--------------------------|
| MC 8 ^a | 20,6 | 0,02 | 5,2 | — | Fok et al. (2012) |
| RSGC 3 | 29,23 | -0,20 | 6 | 16-20 | Clark et al. (2009) |
| Alicante 8 | 24,6 | 0,39 | 6,6 | 16-20 | Negueruela et al. (2010) |
| Alicante 7 | 29,04 | -0,05 | 6 | — | Negueruela et al. (2011) |

^a MC 8 está projetado próximo a Mercer 8, também conhecido como Glimpse 8 (Mercer et al., 2005).

Tabela 3.1: Novos aglomerados abertos na região do par estudado em nosso trabalho.

Na Figura 3.1 mostramos as posições no plano Galáctico dos novos aglomerados abertos da Tabela 3.1, bem como as órbitas e posições atuais do par estudado em nosso trabalho. Podemos ver que, mesmo levando-se em conta os erros de posição, todos distribuem-se ao longo das órbitas que computamos para o nosso par de aglomerados. Fazendo-se as mesmas considerações usadas para o par de aglomerados abertos, a computação das suas órbitas será semelhante às já calculadas, o que reforça a relação entre a passagem de ω Centauri pelo disco Galáctico e o disparo da formação estelar, resultando nos aglomerados mostrados. Adicionalmente pode-se ver um círculo ao redor das posições médias dos aglomerados da Tabela 3.1 e de nosso par de estudo. Este círculo tem raio de 700 parsecs, que é o tamanho do anel de formação estelar estudado em Soria et al. (2004). Desta forma, o presente caso concorda com pelo menos uma observação de efeito semelhante em uma outra galáxia, reforçando o cenário da vinculação da passagem de aglomerados globulares pelo disco Galáctico com o nascimento de aglomerados abertos.

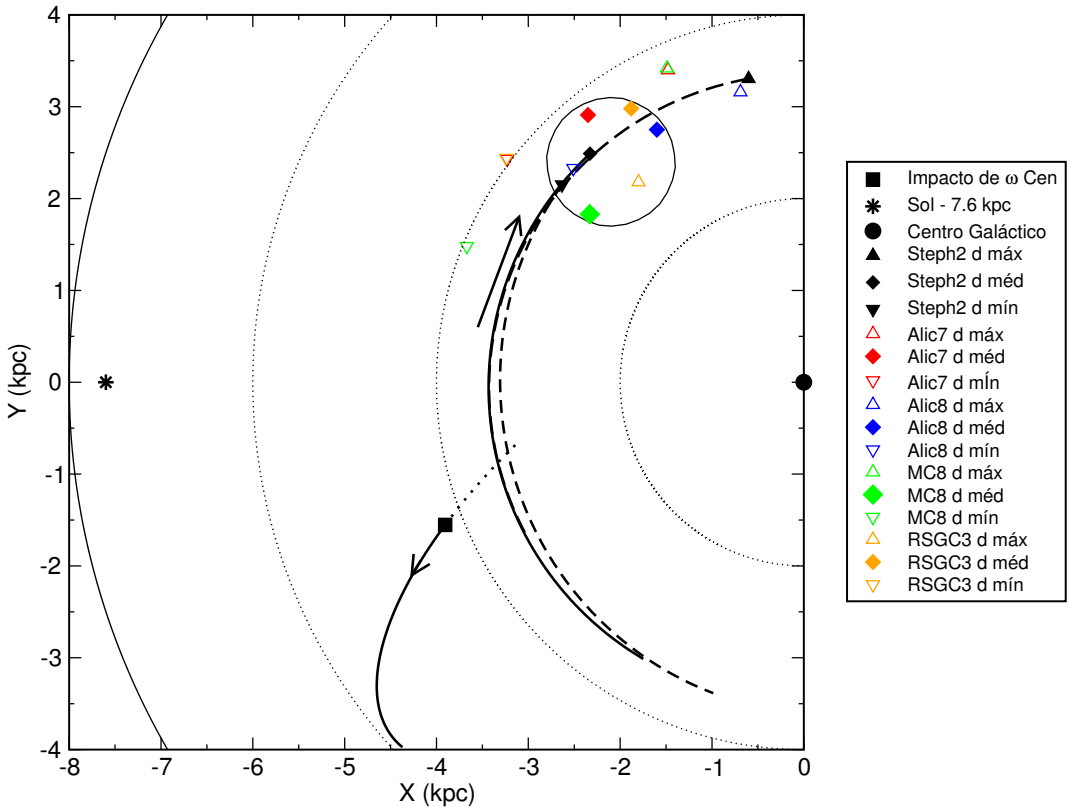


Figura 3.1: Nesta figura vemos as órbitas do par Stephenson 2/BDSB 122 nos últimos 30 milhões de anos, além dos novos aglomerados abertos na mesma região. A parte pontilhada da órbita de ω Centauri indica a porção anterior ao impacto com o disco. Para efeito de comparação o círculo tem um raio de 0,7 Kpc e representa o tamanho da *mini-cartwheel* do estudo de Soria et al. (2004), englobando as posições médias de nosso par e dos novos aglomerados descobertos no entorno. A seta indica o sentido de rotação da Galáxia. *d máx* significa posição média acrescida do erro, *d méd* a posição média e *d mín* a posição média decrescida do erro dos respectivos aglomerados abertos.

Apêndice A

A fossil bulge globular cluster
revealed by VLT multi-conjugate
adaptative optics

A FOSSIL BULGE GLOBULAR CLUSTER REVEALED BY VERY LARGE TELESCOPE MULTI-CONJUGATE ADAPTIVE OPTICS*

SERGIO ORTOLANI¹, BEATRIZ BARBUY², YAZAN MOMANY^{3,4}, IVO SAVIANE³, EDUARDO BICA⁵,
LUCIE JILKOVA^{3,6}, GUSTAVO M. SALERNO⁵, AND BRUNO JUNGWIERT^{7,8}

¹ Dipartimento di Astronomia, Università di Padova, Vicolo dell'Osservatorio 2, I-35122 Padova, Italy; sergio.ortolani@unipd.it

² Instituto de Astronomia, Geofísica e Ciências Atmosféricas da USP, Rua do Matão 1226, São Paulo 05508-900, Brazil; barbuy@astro.iag.usp.br

³ European Southern Observatory, Casilla 19001, Santiago 19, Chile; yommany@eso.org, isaviane@eso.org, ljilkova@eso.org

⁴ Osservatorio Astronomico di Padova, Vicolo dell'Osservatorio 5, I-35122, Padova, Italy

⁵ Departamento de Astronomia, Universidade Federal do Rio Grande do Sul, CP 15051, Porto Alegre 91501-970, Brazil; bica@if.ufrgs.br, salerno@if.ufrgs.br

⁶ Department of Theoretical Physics and Astrophysics, Faculty of Science, Masaryk University, Kotlářská 2, CZ-611 37 Brno, Czech Republic

⁷ Astronomical Institute, Academy of Sciences of the Czech Republic, Bo Ční II 1401/1a, CZ-141 31 Prague, Czech Republic

⁸ Astronomical Institute, Faculty of Mathematics and Physics, Charles University in Prague, Ke Karlovu 3, CZ-121 16 Prague, Czech Republic

Received 2010 June 16; accepted 2011 May 25; published 2011 July 26

ABSTRACT

The globular cluster HP 1 is projected on the bulge, very close to the Galactic center. The Multi-Conjugate Adaptive Optics Demonstrator on the Very Large Telescope allowed us to acquire high-resolution deep images that, combined with first epoch New Technology Telescope data, enabled us to derive accurate proper motions. The cluster and bulge fields' stellar contents were disentangled through this process and produced an unprecedented definition in color–magnitude diagrams of this cluster. The metallicity of $[Fe/H] \approx -1.0$ from previous spectroscopic analysis is confirmed, which together with an extended blue horizontal branch imply an age older than the halo average. Orbit reconstruction results suggest that HP 1 is spatially confined within the bulge.

Key words: Galaxy: bulge – globular clusters: general – globular clusters: individual (HP 1)

Online-only material: color figures

1. INTRODUCTION

A deeper understanding of the globular cluster population in the Galactic bulge is becoming possible, thanks to high-resolution spectroscopy and deep photometry using 8–10 m telescopes. An interesting class concerns moderately metal-poor globular clusters ($[Fe/H] \approx -1.0$), showing a blue horizontal branch (BHB). A dozen of these objects are found projected on the bulge (Barbuy et al. 2009), and they might represent the oldest globular clusters formed in the Galaxy.

According to Gao et al. (2010), the first generation of massive, fast-evolving stars formed at redshifts as high as $z \approx 35$. Second-generation low-mass stars would be found primarily in the inner parts of the present-day Galaxy as well as inside satellite galaxies. Nakasato & Nomoto (2003) suggest that the metal-poor component of the Galactic bulge should have formed through a subgalactic clump merger process in the proto-Galaxy, where star formation would be induced and chemical enrichment occurred by Type II supernovae. The metal-rich component instead would have formed gradually in the inner disk. Therefore, metal-poor inner-bulge globular clusters might be relics of an early generation of long-lived stars formed in the proto-Galaxy.

Another aspect of interest in inner bulge studies comes from evidence that stellar populations in the Galactic bulge are similar to those in spiral bulges and elliptical galaxies, and therefore are of great interest as templates for the study of external galaxies (Bica 1988; Rich 1988). In the past, the detailed study of the bulge globular clusters was hampered by high reddening and crowding. With the improvement of instrumentation, it is now possible to derive accurate proper motions and to apply

membership cleaning. Most previous efforts in proper motion studies were carried out using the *Hubble Space Telescope* (*HST*) data by our group (e.g., Zoccali et al. 2001) for NGC 6553, Feltzing & Johnson (2002) for NGC 6528, and Kuijen & Rich (2002) for field stars, among others.

In a systematic study of bulge globular clusters (e.g., Barbuy et al. 1998, 2009), we identified a sample of moderately metal-poor clusters ($[Fe/H] \sim -1.0$) concentrated close to the Galactic center. HP 1 has a relatively low reddening, and appeared to us as a suitable target to be explored in detail in terms of proper motions. Its coordinates are $\alpha = 17^{\text{h}}31^{\text{m}}05\rlap{.}^{\text{s}}2$, $\delta = -29^{\circ}58'54''$ (J2000), and it is projected at only $3^{\circ}33$ from the Galactic center ($l = -2^{\circ}5748$, $b = 2^{\circ}1151$).

In 2008, the European Southern Observatory (ESO) announced a public call for Science Verification of the Multi-Conjugate Adaptive Optics Demonstrator (MAD; Marchetti et al. 2007), installed at the ESO Melipal (UT3) Telescope. Several star clusters were observed with the MAD facility, delivering high-quality data for the open clusters Trapezium, FSR 1415, and Trumpler 15 (Bouy et al. 2008; Momany et al. 2008; Sana et al. 2010), the globular clusters Terzan 5 and NGC 3201 (Ferraro et al. 2009; Bono et al. 2010), and 30 Doradus (Campbell et al. 2010). The major advantage of MAD is that it allows correcting for atmospheric turbulence over a wide 2' diameter field of view, and as such constitutes a pathfinder experiment for future facilities at the European Extremely Large Telescope (E-ELT). Wide-field adaptive optics with large telescopes open a new frontier in determining accurate parameters for most globular clusters that remain essentially unstudied because of high reddening, crowding (cluster and/or field), and large distances.

In Section 2 the observations and data reductions are described. In Section 3 the HP 1 proper motions are derived. The impact of the high-quality proper motion-cleaned

* The observations were collected with the Very Large Telescope (Melipal) at the European Southern Observatory, ESO, in Paranal, Chile; the run was carried out in Science Demonstration Time.

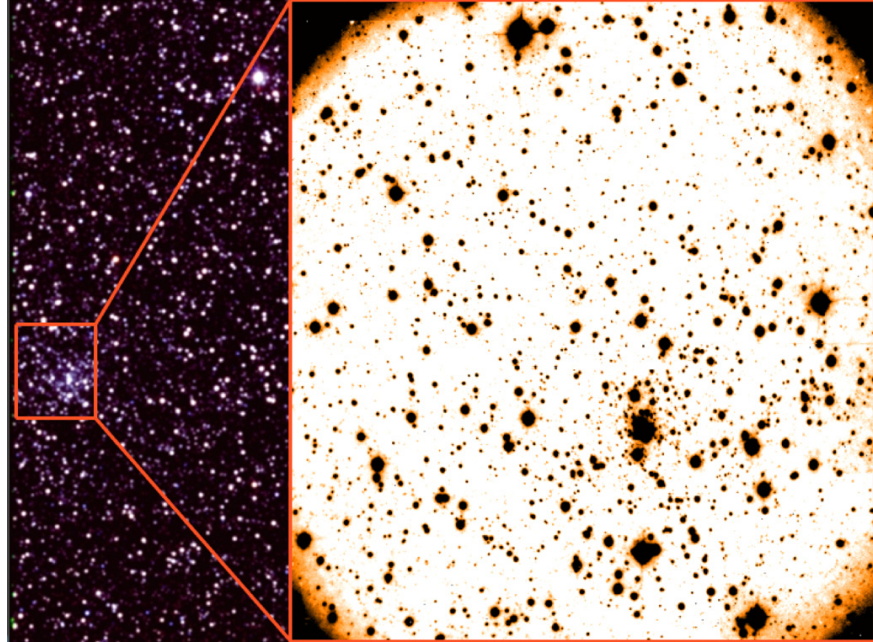


Figure 1. MAD image of the globular cluster HP 1, obtained at ESO-VLT at Paranal, Chile. The left panel is a composite color image of HP 1 from the near-infrared 2MASS survey. The right panel is a close-up of the MAD K -band image covering the central $1.8' \times 1.8'$ of HP 1. North is up and east is to the left. (A color version of this figure is available in the online journal.)

Table 1
 Log of the MAD Observations Obtained on 2008 August 15

| Filter | FWHM | Airmass | DIT (s) | NDIT |
|--------|----------|---------|---------|------|
| K | $0''.19$ | 1.149 | 10 | 30 |
| K | $0''.21$ | 1.179 | 10 | 30 |
| K | $0''.21$ | 1.213 | 10 | 30 |
| K | $0''.27$ | 1.260 | 10 | 30 |
| K | $0''.26$ | 1.304 | 10 | 30 |
| J | $0''.35$ | 1.081 | 10 | 30 |
| J | $0''.41$ | 1.101 | 10 | 30 |
| J | $0''.32$ | 1.124 | 10 | 30 |
| J | $0''.33$ | 1.152 | 10 | 30 |
| J | $0''.42$ | 1.183 | 10 | 30 |

color-magnitude diagrams (CMDs) on cluster properties is examined in Section 4. The clusters’ orbit in the Galaxy is reconstructed in Section 5. Finally, conclusions are given in Section 6.

2. OBSERVATIONS AND DATA ANALYSIS

MAD was developed by the ESO Adaptive Optics Department to be used as a visitor instrument on the Melipal Unit Telescope 3 at the Very Large Telescope (VLT) with a view toward future application to the E-ELT. It was installed at the visitor Nasmyth focus, and the concept of multiple reference stars for layer-oriented adaptive optics corrections was introduced. This allows a much wider and more uniform corrected field of view, providing larger average Strehl ratios and making the system a powerful diffraction limit imager. This is particularly important in crowded fields where photometric accuracy is needed.⁹ Following our successful use of MAD in the first

Science Demonstration (Momany et al. 2008), we were granted time to observe HP 1 in the second Science Demonstration.¹⁰

HP 1 was observed on 2008 August 15. Table 1 displays the log of the J and K_s (for brevity we use K) observations. Clearly, the seeing in K was excellent, being almost half that in J ($0''.23$ versus $0''.38$). The MAD infrared scientific imaging camera is based on a 2048×2048 pixel HAWAII-2 infrared detector with a pixel scale of $0''.028$. In total, 25 minutes of scientific exposures were dedicated to each filter, and subdivided into five dithered images.

The images were dark and sky-subtracted, and then flat-fielded following the standard near-infrared recipes (e.g., Momany et al. 2003), within the IRAF environment. The typical dithering pattern of a MAD observation allows a field of view of $\sim 2'$ in diameter. Within this field of view, three reference bright stars (R magnitudes that ranged between 12.5 and 13.8 according to their magnitudes in the second US Naval Observatory CCD Astrograph Catalog (UCAC2)) were selected to ensure the optics correction. However, one of these proved to be a blend of two stars, which did not allow a full optical correction of the field.

Figure 1 shows the mosaic of all 10 J and K images as constructed by the DAOPHOT/MONTAGE2 task. The superb VLT/MAD resolution is illustrated when compared to that seen in the Two Micron All Sky Survey (2MASS) K image of HP 1. For proper motion purposes, the MAD data set represents our second epoch data. The displacement of the HP 1 stellar content was derived by comparing the position of the stars in this data set with respect to that obtained with the SUSI CCD camera at the New Technology Telescope (NTT) on 1994 May 16 (Ortolani et al. 1997). The epoch separation is 14.25 yr. It is

⁹ <http://www.eso.org/projects/aot/mad/>

¹⁰ <http://www.eso.org/sci/activities/vltv/mad/>

THE ASTROPHYSICAL JOURNAL, 737:31 (9pp), 2011 August 10

ORTOLANI ET AL.

worth emphasizing that the seeing of $0''.45$ for the first epoch V image of HP 1 is one of the best obtained with NTT (Ortolani et al. 1995, 1997).

The photometric reductions of the two data sets (NTT and MAD) were carried out separately. We found about 3100 stars in common between the MAD and NTT data, which were used for proper motion analyses.

2.1. Photometric Reduction and Calibration

The stellar photometry and astrometry were obtained by point-spread function (PSF) fitting using DAOPHOT II/ALLFRAME (Stetson 1994). Once the FIND and PHOT tasks were performed and the stellar-like sources were detected, we searched for isolated stars to build the PSF for each single image. The final PSF was generated with a PENNY function that had a quadratic dependence on frame position. ALLFRAME combines PSF photometry carried out on the individual images and allows the creation of a master list by combining images from different filters. This pushes the detection limit to fainter magnitudes and provides better determination of the stellar magnitudes (given that five measurements were used for each detected star).

Our observing strategy employed the same exposure time for all images, and no bright red giant stars were saturated. When producing the photometric catalog in one filter (and since only the central part of the field of view had multiple measurements of any star), stars appearing in any single image were considered to be real. Later, when producing the final JK color catalog, only those appearing in both filters were recorded (this way we essentially removed all detections due to cosmic rays and other spurious detections). The photometric catalog was finally transformed into coordinates with astrometric precision by using 12 UCAC2 reference stars¹¹ with $R \leq 16.2$.

Photometric calibration of the J and K data has been made possible by a direct comparison of the brightest MAD nonsaturated ($8.0 \leq K \leq 13.0$) stars with their 2MASS counterpart photometry. From these stars we estimate a mean offset of $\Delta J_{\text{MAD}-\text{J@2MASS}} = -3.157 \pm 0.120$ and $\Delta K_{\text{MAD}-\text{K@2MASS}} = -1.395 \pm 0.134$.

Photometric errors and completeness were estimated from artificial star experiments previously applied to similar MAD data (Momany et al. 2008). The images with added artificial stars were reprocessed in the same manner as the original images. The results for photometric completeness showed that we reach a photometric completeness of $\sim 75\%$, 50% , and 10% around $K \simeq 17.0$, 17.5 , and ~ 18.0 , respectively.

3. DERIVATION OF THE PROPER MOTIONS

The proper motion of the HP 1 stellar content was derived by estimating the displacement in the (x, y) instrumental coordinates between the MAD (second epoch) data and the NTT (first epoch) data. Since this measurement was made with respect to reference stars that are cluster members, the motion zero point is the centroid motion of the cluster. The small MAD field of view is fully sampled by the wider NTT coverage, and thus essentially all MAD entries had NTT counterparts for proper motion determination. In this regard, we note that the photometric completeness of the MAD data set is less than that of the optical V, I NTT data that reached at least two magnitudes below the cluster turnoff (Ortolani et al. 1997).

¹¹ <http://www.usno.navy.mil/USNO/astrometry/optical-IR-prod/ucac>

The DAOPHOT/DAOMASTER task was used to match the photometric MAD and NTT catalogs, using their respective (x, y) instrumental coordinates. This task employed a cubic transformation function, which, with a matching radius of 0.5 pixels or $0''.015$, easily identified reference stars among the cluster's stars (having similar proper motions). As a consequence, the stars that matched between the two catalogs were basically only HP 1 stars. In a separate procedure, the J2000 MAD and NTT catalogs, transformed into astrometric coordinates, were applied to a matching procedure using the IRAF/TMATCH task. This first/second epoch merged file also included the (x, y) instrumental coordinates of each catalog. Thus, applying cubic transformation to both coordinate systems yielded the displacement with respect to the centroid motion of HP 1. An extraction within a 1.5 pixel radius around $(0, 0)$ in pixel displacement was shown to contain most, and essentially only, HP 1 stars, and we will use this selection for the rest of the paper.

On the other hand, stars outside this radius (i.e., representing the bulge populations) are more dispersed and required a careful analysis. In a first attempt, we used only the stars with $\Delta y < -1$ (in order to avoid cluster stars) to get the barycentric position of the field bulge population in x , and stars with $\Delta x > 1$ to measure the field bulge population in y . After a number of tests with different selections, in a second attempt we made a two-Gaussian component fit along a 0.2 pixel-wide strip connecting the center of the cluster distribution and the field distribution. For the present analysis, we adopted relative to the field the mean of the two determinations $(\Delta x, \Delta y) = (-2.1, 1.96)$ for the proper motion of the cluster. From the Gaussian fit we derived the width of the distributions of the cluster and field stars, resulting, respectively, in $\sigma = 0.583$ and 2.565 pixels, corresponding to 15 and 41 mas, respectively. This is the error of the single star position. The statistical error of the mean is obtained by dividing the single star error by the square root of the number of stars used (about 1700 in the cluster and 1500 in the bulge) for each of the two measurements. The error in the mean position of the field obviously dominates and corresponds to about 0.05 pixels, or 1.3 mas (about 0.1 mas yr $^{-1}$). This is indeed a very small error. We performed a number of tests fitting the cluster stars and the field stars in different conditions checking for additional uncertainties. A further quantitative evaluation of the fitting uncertainty can be obtained by measuring the different distances between the centers of the HP 1 proper motion cloud to that of the field, propagated from the error on the angle of the line connecting the two groups of stars. The angle of the vector joining the center of the HP 1 proper motion cloud to that of each star of the bulge was computed, and a Gaussian fit was performed, which returned a 1σ dispersion of 14° . This uncertainty propagates over the distances of the two groups by about 0.39 mas yr $^{-1}$, dominating over the other discussed sources.

3.1. Astrometric Errors

The astrometric errors are the combination of different random and systematic errors. Anderson et al. (2006) concluded that in the case of relative ground-based astrometry in a small rich field, the main error sources are random centering errors due to noise and blending, random-systematic errors due to field distortions, and systematic errors due to chromatic effects.

1. *Centering errors.* Considering that we used two very different data sets—a first epoch based on direct CCD photometry, and a second one on the corrected infrared adaptive

THE ASTROPHYSICAL JOURNAL, 737:31 (9pp), 2011 August 10

ORTOLANI ET AL.

optics (with a much wider scale and better resolution)—we can assume that the astrometric random errors are dominated by the first epoch classical CCD photometry. Following Anderson et al. (2006), we performed a test with three consecutive NTT images of Baade’s Window taken in the same night. They were obtained with equal (four-minute) exposure times, and nearly at the same pixel positions. The seeing was stable and these images were obtained about 1 hr later than the 10 minute cluster V exposure.

This Baade’s Window field was chosen because the stars are uniformly distributed across the image, and the density of stars is similar to the HP 1 field. These images were analyzed in Ortolani et al. (1995). The position of the stars in common was compared. The photometric and astrometric errors are shown in Figure 2. The astrometric centering error, averaged over the whole dynamic range, is 0.1 pixels, as indicated in Figure 2. This corresponds to 13 mas, which is comparable with the 7 mas pointing error by Anderson et al. (2006). The value of 13 mas amounts to 0.91 mas yr^{-1} in an interval of 14.25 yr. Taking into account the number of about 3000 stars (half field and half cluster) used for the proper motion derivation of HP 1, this leads to a minor error of $0.022 \text{ mas yr}^{-1}$.

2. *Field distortion errors.* The field distortion analysis is usually performed employing shifted images of a field with uniformly distributed stars. HP 1 multiple shifted images are not available in our first epoch run. To estimate the distortions, we compared the proper motion of cluster stars in HP 1 NTT images as a function of the distance from the optical center. The distribution did not show any relevant trend, and the statistical analysis indicates that there is no significant shift above 0.01 pixels across the field. This corresponds to 0.19 mas yr^{-1} .

3. *Chromatic errors.* Chromatic errors are due to the different refraction, both atmospheric and instrumental, on stars with different colors. The refraction dependence on wavelength (inverse quadratic to the first approximation) makes this effect more pronounced in the color ($V - I$) than in the near-infrared.

Ideally, a chromatic experiment should include a measurement of the displacement of stars with different colors at different air masses. However, we do not have specific observations for this test. Thus, we followed the procedure given by Anderson et al. (2006), where they measured the displacement of stars as a function of their colors. We took the resulting pixel displacement of the cluster stars and separately checked the shift variations with the color ($V - I$). Such a plot does not show an evident dependence on color. This is expected since our NTT observations were taken very close to the zenith (air mass ~ 1.04), and the infrared MAD data have a negligible effect.

In order to further quantify any chromatic systematic effect, we subdivided the sample of cluster stars into redder ($V - I > 2.2$) and bluer ($V - I < 2.2$) groups, of 106 and 171 stars, respectively. The displacement between the two groups resulted is 0.031 ± 0.03 pixels, corresponding to 0.9 mas . For 14.25 yr, this gives 0.06 mas yr^{-1} .

4. *Total errors.* By quadratically adding the errors on centering, distortion, and chromatic effects of, respectively, $0.022 \text{ mas yr}^{-1}$, 0.19 mas yr^{-1} , and 0.06 mas yr^{-1} , a total contribution of these errors of 0.2 mas yr^{-1} is obtained.

The estimated error of 0.39 mas yr^{-1} in the proper motion value indicates that the effect due to the mutual field and

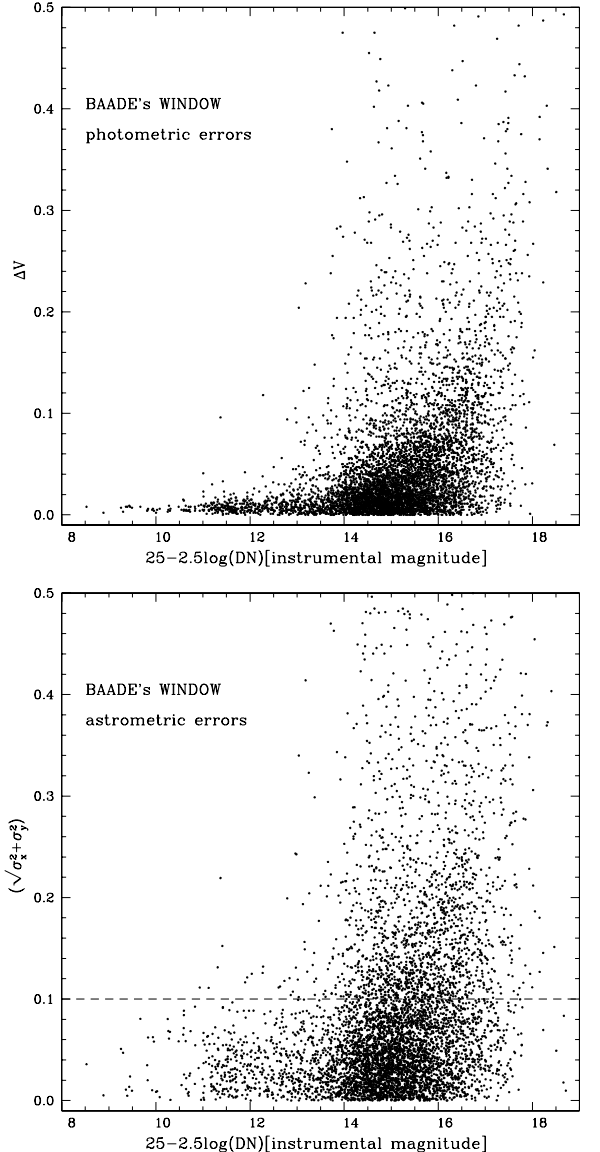


Figure 2. Photometric and astrometric errors of Baade’s Window images. Top panel: photometric errors ΔV vs. instrumental magnitude. The dashed line shows the average astrometric error. Bottom panel: astrometric error in the NTT pixel scale vs. instrumental magnitude.

cluster star contamination dominates over the astrometric pointing, distortion, and chromatic errors.

4. THE PROPER MOTION-CLEANED COLOR-MAGNITUDE DIAGRAM OF HP 1

Figure 3 presents the MAD K versus $J - K$ CMDs showing the proper motion decontamination process in three panels: the whole field, the cluster proper motion decontaminated, and the remaining field only. In the top panels the displacements of stars between the NTT and MAD images are shown, plotted in the MAD pixel scale.

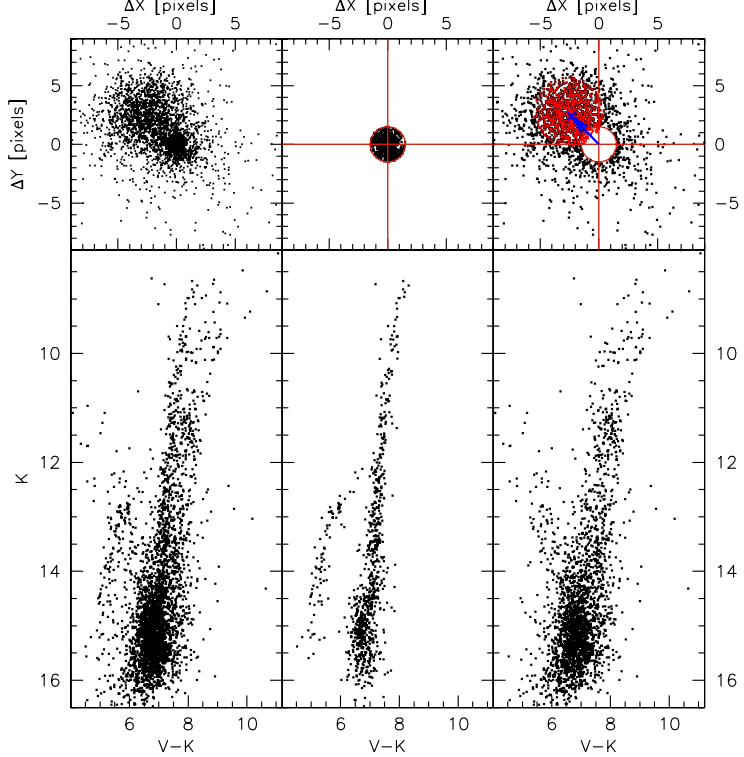


Figure 3. HP 1: proper motion decontaminated K vs. $J - K$ CMD. Top left panel: displacement of NTT (first epoch)–MAD (second epoch), plotted in the MAD pixel scale. Top middle panel: the cluster sample is encircled and l, b directions are indicated by the arrows. Top right panel: field sample only. Bottom left panel: observed CMD. Bottom middle panel: proper motion decontaminated cluster CMD. The two stars indicated as red squares are the two giant stars analyzed with high-resolution spectroscopy. Bottom right panel: remaining field star CMD. The extraction is within a 1.5 pixel radius.

(A color version of this figure is available in the online journal.)

The decontaminated cluster CMD provides fundamental parameters for studying its properties, in particular metallicity and age. Figure 4 shows a J versus $V - K$ proper motion decontaminated CMD of HP 1. A distance modulus of $(m - M)_J = 15.3$ and a reddening of $E(V - K) = 3.3$ are applied, and a Padova isochrone (Marigo et al. 2008) with metallicity $Z = 0.002$ and an age of 13.7 Gyr is overplotted. The fit confirms the cluster metallicity of $[Fe/H] = -1.0$, found from high-resolution spectroscopy (Barbuy et al. 2006). We note that the turnoff is not as well matched as the giant branch, due to two well known main reasons: the bluer turnoff in isochrones relative to observations is possibly connected with color transformations, and systematic bias in the photometric errors gives brighter magnitudes close to the limit of the photometry. Similarly, Figure 5 displays the K versus $V - K$ HP 1 diagram as compared with the NGC 6752 ($[Fe/H] = -1.42$) mean locus (Valenti et al. 2004). The red giant branches of M30, M107, 47 Tuc, and NGC 6441 of metallicities $[Fe/H] = -1.91, -0.87, -0.70$, and -0.68 , respectively, are also overplotted with metallicity values, mean loci, and red giant fiducials from Valenti et al. (2004). The HP 1 bright red giants clearly overlap with the M107 fiducial (reflecting their similar metallicity values) and are redder with respect to the NGC 6752 bright giants. On the other hand, the cluster's old age is reflected by the presence of a well defined and extended BHB (very similar to NGC 6752). Five RR Lyrae candidates appear in the RR Lyrae gap, at $4.2 \leq (V - K) \leq 5.0$.

Terzan (1964a, 1964b, 1965, 1966) reported 15 variable stars in HP 1 but none has been identified as RR Lyrae. The Horizontal Branch (HB) morphology is sensitive mainly to metallicity and age. The age effect is related to the so-called second parameter effect (Sandage & Wildey 1967), also demonstrated in models by Lee et al. (1994), Rey et al. (2001), and in observations by Dotter et al. (2010). In particular, Dotter et al. (2010) analyzed the HB morphology from Advanced Camera for Surveys/HST observations, based on the difference between the average HB $V - I$ color and the subgiant branch (SGB) color $\Delta V - I_{\text{HB}}^{\text{SGB}}$, and concluded that age dominates the second parameter. This indicator is very sensitive to the cluster age, and more so around the metallicity $Z = 0.002$.

For HP 1 the mean $V - I$ color difference between the SGB and the HB is $\Delta V - I_{\text{HB}}^{\text{SGB}} = 0.75 \pm 0.01$. A comparison with Dotter et al.'s (2010) sample shows that HP 1 has a very blue HB for its metallicity. We selected five clusters with the same HB morphological index and found an average metallicity of $[Fe/H] = -1.9 \pm 0.36$. We also selected another group of five clusters with a comparable metallicity to HP 1. This second group has an average $\Delta V - I = 0.46 \pm 0.27$, which is considerably smaller than in HP 1, consistent with HP 1 having a much bluer HB. Both cluster groups have a mean age of 12.7 ± 0.4 Gyr. From Figure 17 of Dotter et al. (2010), we get an age difference of about 1 Gyr older for HP 1 relative to their sample of halo clusters with ~ 12.7 Gyr, resulting in an age of

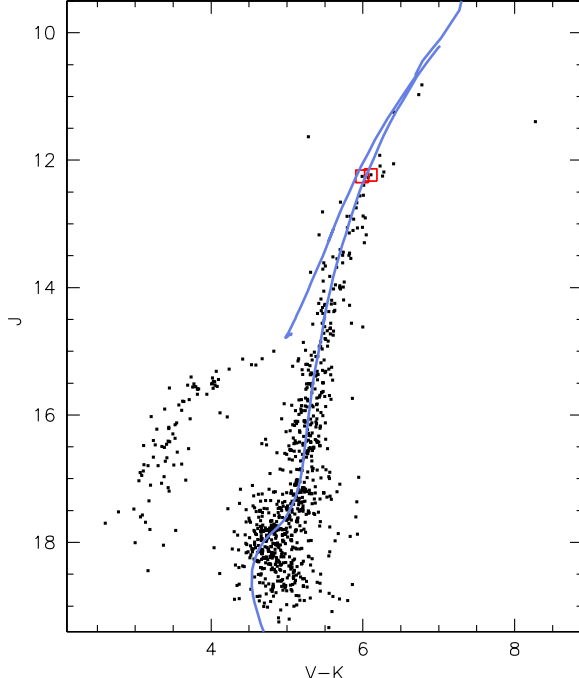


Figure 4. HP 1: J vs. $V - K$ CMD, built from a proper motion selected subsample of stars. The extraction is within a 1.5 pixel radius, in pixel displacement. A Padova isochrone of $Z = 0.002$ and an age of 13.7 Gyr are overplotted on the observed CMD. A distance modulus of $(m - M)_J = 15.3$ and a reddening of $E(V - K) = 3.3$ were adopted. The metallicity, distance, and reddening adopted for the fit are in agreement with the spectroscopic analysis carried out for two stars indicated by squares (Barbuy et al. 2006). The present MAD photometry reaches the turnoff limit.

(A color version of this figure is available in the online journal.)

~13.7 Gyr for HP 1. Therefore, HP 1 appears to be among the oldest globular clusters in the Galaxy.

For the distance determination, there are basically two methods: (1) the relative distance between the cluster and bulk of the bulge field, and (2) based on the absolute distance, which requires reddening values. For the first of these methods, we rely on the difference between the HP 1 HB at the RR Lyrae level, at $V = 18.7$, and that of the bulge field at $V = 19.35$. Thus, the cluster is $\Delta V = 0.66$ brighter than the field, and taking into account metallicity effects on the HB luminosity (Buonanno et al. 1989), we obtain $\Delta V = 0.35 \pm 0.14$. This implies that the cluster is 1.2 ± 0.4 kpc in the foreground of the bulge bulk population. The uncertainty is due to the metallicity difference of about 1 dex between the bulge ($[Fe/H] \approx 0.0$) and HP 1 ($[Fe/H] \approx -1.0$). Assuming the distance of the Galactic center to be $R_{GC} = 8.0 \pm 0.6$ (Majaess et al. 2009; Vanhollebeke et al. 2009), a distance of $d_\odot = 6.8$ kpc is obtained. If the orbits of stars near the super massive black hole near the Galactic center are used, a distance of $R_{GC} = 8.33 \pm 0.35$ kpc is given by Gillessen et al. (2009). In this case the distance of HP 1 to the Sun is $d_\odot = 7.1$ kpc. This relative distance method is reddening-independent, because the reddening of the cluster and surrounding field is expected to be essentially the same, due to a negligible reddening inside the bulge (Barbuy et al. 1998). Therefore, the distance of the cluster to the Galactic center depends only on the assumed distance of the Galactic center.

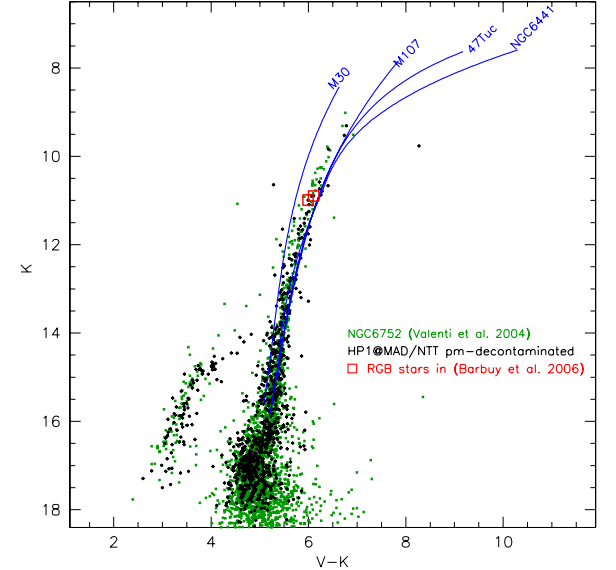


Figure 5. K vs. $V - K$ HP 1 diagram (black dots) compared with the NGC 6752 (green dots) catalog (Valenti et al. 2004). We assumed the fiducial values $(m - M)_0 = 13.18$, $E(B - V) = 0.04$, $A_V = 3.1$, $A_K = 0.38$. Also plotted are the red giant branches of comparison Galactic globular clusters (blue lines): M30, M107, 47 Tuc, and NGC 6441 ($[Fe/H] = -2.12, -1.04, -0.76$, and -0.68 ; the catalog and the red giant fiducials are from Valenti et al. 2004). The HP 1 bright red giants are clearly overlapping with the M107 fiducial (reflecting their similar metallicity) and are redder with respect to the NGC 6752 bright giants. (A color version of this figure is available in the online journal.)

The second method of absolute distances requires reddening determinations. From the optical and infrared CMDs, and adopting the absolute-to-selective absorption $R_V = 3.2$ (Barbuy et al. 1998), we obtain a mean distance from the Sun of $d_\odot = 7.3 \pm 0.5$ kpc. Within the uncertainties for the cluster and Galactic center distances, we conclude that HP 1 is probably the globular cluster located closest to the Galactic center.

For simplicity, we assume the distance of HP 1 from the Sun to be $d_\odot = 6.8$ kpc hereafter.

5. SPATIAL MOTION OF HP 1 IN THE GALAXY

5.1. Absolute Proper Motion

To compute the velocity components of HP 1's motion, we need its radial velocity and the proper motion. The heliocentric radial velocity $v_r^{\text{hel.}} = 45.8 \pm 0.7$ km s $^{-1}$ was adopted from the high-resolution analysis by Barbuy et al. (2006). The proper motion can be computed with respect to the bulge, and the bulge proper motion can then be subtracted. The bulge proper motion is a composition of the bulge internal kinematics and the reflected motion of the LSR. Near the position of HP 1, the bulge kinematics are close to that of a rotating solid body with a spin axis orthogonal to the Galactic plane (e.g., Zhao 1996). Note also that this correction is not large: HP 1 is projected so close to the Galactic center that the rotational velocity of the bulge is closely aligned with the line of sight, so its tangential component is very small. Because both motions are parallel to the Galactic plane, it is convenient to work in Galactic coordinates.

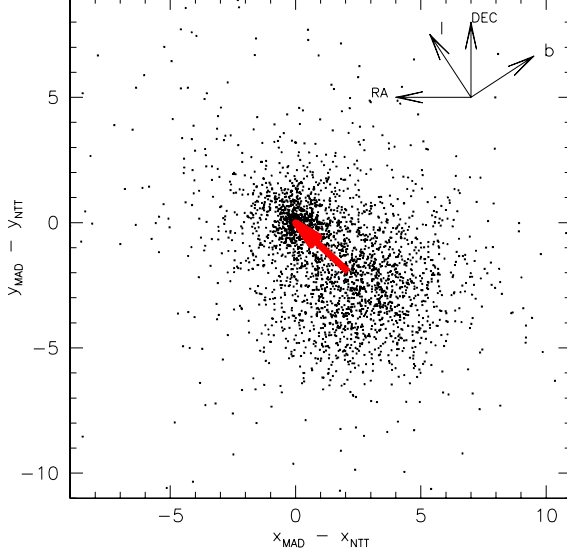


Figure 6. In the reference system $(\Delta x, \Delta y) = (x_{\text{MAD}} - x_{\text{NTT}}, y_{\text{MAD}} - y_{\text{NTT}})$ with origin in HP 1 the bulge has the coordinates $(2.10, -1.96)$. Therefore, the HP 1 motion with respect to the bulge has the vector $\vec{u}_{\text{px}}^* = (-2.10, 1.96)$ (red arrow). Because R.A. and Δx have opposite directions, the vector expressed in equatorial coordinates is $\vec{u}_{\text{Eq}}^* = (0'.0588, 0'.05488)$. The relative orientation of the equatorial and Galactic coordinate systems is shown in the upper right corner, making clear that the proper motion of HP 1 is mostly along positive l , with a small component along negative b . The orbit must therefore be confined near the Galactic plane.

(A color version of this figure is available in the online journal.)

As Figure 6 shows, the HP 1 motion with respect to the bulge has a vector $\vec{u}_{\text{px}}^* = (-2.10, 1.96)$ pixels.¹²

To estimate the bulge internal motion, we note that Tiede & Terndrup (1999) obtained a rotational velocity of $\sim 75 \text{ km s}^{-1}$ in their fields 6/05 and 6/18 ($b = -6^\circ$ and the respective field numbers), at positions $l = -8^\circ 7$ and $l = 8^\circ 4$, respectively. In the solid body approximation, v_{rot} depends linearly on the radius r (confirmed by Howard et al. 2008), and at the position of HP 1 (Section 1) we expect $v_{\text{rot}} \simeq 75 \text{ km s}^{-1} / 8^\circ 5 \times 2^\circ 58 = 22.8 \text{ km s}^{-1}$ (where we assumed $l \propto r$ for small values of l). Basically the same value (22.7 km s^{-1}) is predicted at a distance of 0.38 kpc ($= r_\odot \times \sin 2^\circ 58$ with $r_\odot = 8.4 \text{ kpc}$) by the angular velocity of $60.0 \text{ km s}^{-1} \text{ kpc}^{-1}$ adopted in our model (Section 5.2). Assuming that bulge stars are at the distance of the Galactic center, the tangential component of v_{rot} is $v_T = 22.8 \text{ km s}^{-1} \times \sin 2^\circ 58 / \cos 2^\circ 58 = 1.03 \text{ km s}^{-1}$

¹² Note that in Section 3 we were working with NTT–MAD coordinates, while here we put the two epochs in chronological order, thus MAD–NTT coordinates are used. The signs are therefore inverted. Taking into account the scale of $0''.028 \text{ pixel}^{-1}$ and that $\Delta \text{R.A.} = -\Delta x$, the vector expressed in equatorial coordinates is $\vec{u}_{\text{Eq}}^* = (0'.0588, 0'.05488)$. The position angle of the b -axis with respect to the decl. axis is $-56^\circ 745$, which can be used to rotate \vec{u}_{Eq}^* , obtaining $\vec{u}_{\text{Gal}} = (\Delta l, \Delta b)$ with $\Delta l = 0'.0781 \pm 0'.0056$ and $\Delta b = -0'.0191 \pm 0'.0056$. The coordinate transformations were performed with the code SM (Lupton & Monger 1997) using the *project* package, written by M. Strauss and R. Lupton. With an epoch difference of $\Delta t = 14.2519 \pm 0.0027 \text{ yr}$, these displacements yield proper motion components relative to the bulge of $\mu_l^{\text{rel}} \times \cos b \simeq 5.5 \text{ mas yr}^{-1}$ and $\mu_b^{\text{rel}} \simeq -1.34 \text{ mas yr}^{-1}$. As recalled above, to obtain absolute proper motions we subtract the reflected motion of the LSR and the bulge internal motion. Assuming $V_{\text{LSR}} = -243 \text{ km s}^{-1}$, at a distance of 8.4 kpc from the Galactic center (these values are explained below) we obtain $(\mu_l, \mu_b)_{\text{LSR}} \simeq (6.102, 0) \text{ mas yr}^{-1}$.

directed toward increasing l . After adding v_T to V_{LSR} , the composite motion of the bulge becomes $(\mu_l, \mu_b)_{\text{bulge+LSR}} = (6.127, 0) \text{ mas yr}^{-1}$, and subtracting it from the relative motion quoted above for HP 1 yields $\mu_l \times \cos b = -0.65 \pm 0.39 \text{ mas yr}^{-1}$ and $\mu_b = -1.34 \pm 0.39 \text{ mas yr}^{-1}$. Using this proper motion, in the next section we calculate the cluster orbit.

5.2. HP 1's Orbit in the Galaxy

The orbit of HP 1 was computed both with the axisymmetric model by Allen & Santillan (1991) and with a model including a bar. The models and integration algorithm are described by L. Jilkova et al. (2011, in preparation). Similar models were used in Magrini et al. (2010). Compared to these earlier versions, the axisymmetric model was rescaled to match the more recent values of rotation velocity, solar Galactocentric distance, and solar velocity relative to the LSR. Reid et al. (2009) estimated a rotation velocity of $254 \pm 16 \text{ km s}^{-1}$ and a distance of $8.4 \pm 0.6 \text{ kpc}$, using the solar motion relative to the LSR determined by Dehnen & Binney (1998). However, the analysis of Dehnen & Binney was recently reexamined by Schönrich et al. (2010) who obtained slightly different values—the component in the direction of solar Galactic rotation was found to be 7 km s^{-1} higher. Taking this into account, we rescaled the Allen & Santillan (1991) parameters to get values of 243 km s^{-1} at 8.4 kpc , which is also consistent with the results of Reid & Brunthaler (2004), who obtained the solar rotation velocity from the proper motion of Sgr A*.

The Galactic bar is modeled by a Ferrers potential of an inhomogeneous triaxial ellipsoid (Pfenniger 1984). The model parameters are adopted from Pichardo et al. (2004) with a length of 3.14 kpc , an axis ratio of $10:3.75:2.56$, a mass of $0.98 \times 10^{10} M_\odot$, an angular velocity of $60.0 \text{ km s}^{-1} \text{ kpc}^{-1}$, and an initial angle with respect to the direction toward the Sun of 20° (in the direction of Galactic rotation). For the axisymmetric background, we keep the potential described above with decreased bulge mass near the mass of the bar.

The initial conditions for the orbit calculations are obtained from the observational data characterizing the cluster: coordinates, distance to the Sun, radial velocity, and proper motion. To evaluate the impact of the measurement errors, we calculate a set of 1000 orbits with initial conditions given by sampling the distributions of observational inputs. We assume normal distributions for the distance to the Sun, radial velocity, and proper motion. The errors on radial velocity and proper motion components are given above, while for the distance to the Sun we assumed an error of 10%.

The transformation of the observational data to the Cartesian coordinate system centered on the Sun was carried out with the Johnson & Soderblom (1987) algorithm. The velocity vector with respect to the LSR is then obtained by correcting for the solar motion with respect to the LSR from Schönrich et al. (2010): $(U, V, W)_\odot = (11.1, 12.24, 7.25) \text{ km s}^{-1}$ (right-handed system, with U in the direction toward the Galactic center and V in the Galactic rotation direction). The final transformation to the Galactocentric coordinate system was made by using a solar Galactocentric distance of 8.4 kpc and a LSR rotation velocity of 243 km s^{-1} (see above). We obtain proper motions in equatorial coordinates $\mu_{\text{RA}} \times \cos \text{DEC} = 0.76 \pm 0.39 \text{ mas yr}^{-1}$ and $\mu_{\text{DEC}} = -1.28 \pm 0.39 \text{ mas yr}^{-1}$, and Cartesian coordinates and velocities $(x, y, z) = (1.59, 0.31, 0.25) \text{ kpc}$ and $(v_x, v_y, v_z) = (-57.47, -231.99, -34.26) \text{ km s}^{-1}$. We adopted

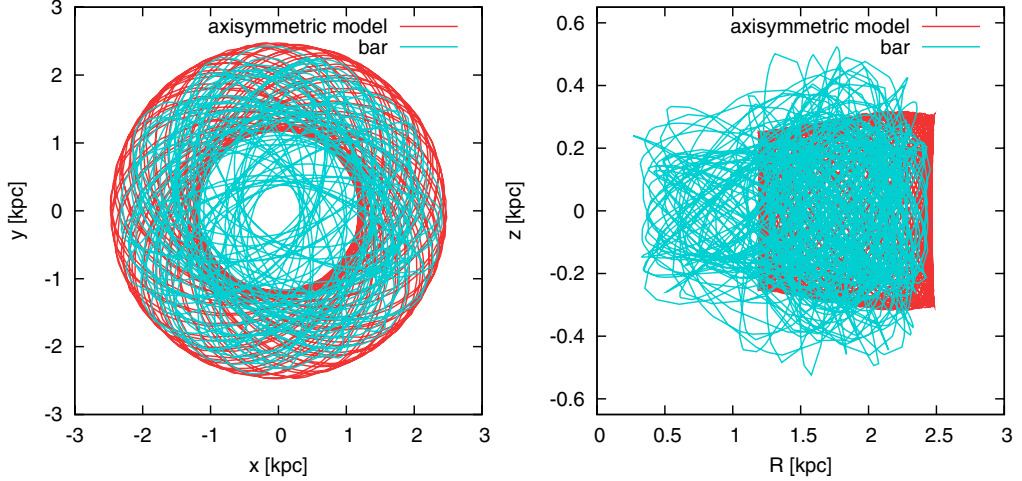


Figure 7. Galactic orbit of the cluster. Projections into the Galactic and meridional planes are plotted in the left and right panels, respectively. Orbit in the axisymmetric model is plotted by the red line and the orbit in the model including a bar by the blue line. Initial conditions are given by mean observational input data; see the text for a detailed description of integrations.

(A color version of this figure is available in the online journal.)

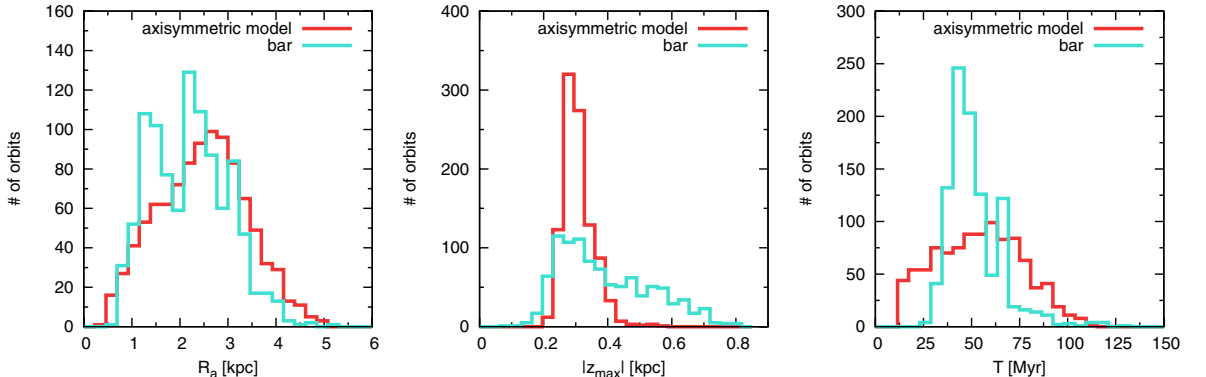


Figure 8. Distributions of orbital parameters—apogalacticon R_a , vertical height of orbit $|z_{\max}|$, and phase period T . Distributions given by the axisymmetric model are plotted by the red line and in the model with a bar by the blue line (same as in Figure 7).

(A color version of this figure is available in the online journal.)

a right-handed, Galactocentric Cartesian system (x toward the Sun direction, z toward the north Galactic pole).

We integrate the orbits with such initial conditions backward for an interval of 3 Gyr using a Bulirsch–Stoer integrator with adaptive time step (Press et al. 1992). An example of orbits given by the average values of the observational data is given in Figure 7. The presence of the bar disturbs the orbit of this central globular cluster, causing deviations not found in the axisymmetric model. This can be considered as an upper limit for the excursions that the cluster can make inward and outward. Even so, it is clear that the cluster is essentially confined within the bulge.

Running simulations for a longer time is not very meaningful because there is evidence that the bar structure is a transient feature. For example, Minchev et al. (2010) suggest that the current bar might have formed only 2 Gyr ago. It is impossible to simulate the orbit along the entire life of the Milky Way, but one can guess that older bars would have had a similar effect on the orbit of HP 1. Note that we also included the spiral arms, but

they do not change the orbit significantly. They are very weak and the orbit is too close to the Galactic center to be influenced by any radial migration due to bar and spiral arm interaction.

We calculated orbital parameters as averaged values over individual revolutions in the Galactic plane for each orbit. Distributions for apogalacticon R_a , vertical height of orbit $|z_{\max}|$, and phase period T are shown in Figure 8. In general, the orbits do not reach galactic distances larger than 5 kpc and the cluster remains close to the Galactic plane ($|z_{\max}| < 0.3$ kpc for the axisymmetric model, $|z_{\max}| < 0.6$ kpc for the model including the bar).

For comparison purposes, we also computed the HP 1 orbit using the code developed by Mirabel et al. (2001) that includes the Galactic spheroidal and the disk potentials. It was recently applied to ω Centauri orbital simulations (Salerno et al. 2009). By this method we essentially use the same initial conditions (U_0, V_0, W_0) as in the method described above, and the simulation results agreed well with the previous method for the barless model.

THE ASTROPHYSICAL JOURNAL, 737:31 (9pp), 2011 August 10

ORTOLANI ET AL.

6. CONCLUSIONS

The clear definition of an extended BHB morphology obtained from these high spatial resolution data, as provided using the proper motion cleaning method, indicates a very old age for HP 1 of ~ 1 Gyr older than the halo average.

The proper motions and orbits derived indicate that HP 1 does not wade into the halo and is confined within the Galactic bulge. As a result, HP 1 can be identified as a representative relic of an early generation of star clusters formed in the proto-Galaxy. The very old globular cluster NGC 6522, also having moderate metallicity and a BHB, is also confined within the bulge (Terndrup et al. 1998). Compared with the template metal-rich bulge globular cluster NGC 6553 (Zoccali et al. 2001; Ortolani et al. 1995), HP 1 appears to have a more eccentric orbit, and it is much closer to the Galactic center.

Extensive tests of orbits within potential wells that include massive bars show that the confinement of HP 1 within the bulge is maintained even in the case of random orbits generated by the presence of the bar.

The case of HP 1, revealed using wide-field multi-conjugate adaptive optics, shows that such ground-based facilities can be used for high spatial resolution studies of crowded inner bulge clusters. Such data can provide a much better understanding of globular cluster subsystems, their connection with stellar populations in the Galaxy, and the sequence of processes involved in the formation of the Galaxy itself.

We are grateful to Ata Sarajedini for helpful discussions on the second parameter effect. We thank the referee for important suggestions on the proper motion analysis. We thank the ESO Adaptive Optics group, in particular, Enrico Marchetti and Paola Amico. B.B. and E.B. acknowledge grants from the Brazilian agencies CNPq and FAPESP. S.O. acknowledges the Italian Ministero de l'Università e della Ricerca Scientifica e Tecnologica.

REFERENCES

- Allen, C., & Santillan, A. 1991, RevMexAA, **22**, 255
 Anderson, J., Bedin, L. R., Piotto, G., Yadav, R. S., & Bellini, A. 2006, A&A, **454**, 1029
 Barbuy, B., Bica, E., & Ortolani, S. 1998, A&A, **333**, 117
 Barbuy, B., Zoccali, M., Ortolani, S., Hill, V., Minniti, D., Bica, E., Renzini, A., & Gomez, A. 2009, A&A, **507**, 405
 Barbuy, B., et al. 2006, A&A, **449**, 349
 Bica, E. 1988, A&A, **195**, 76
 Bono, G., et al. 2010, ApJ, **708**, L74
 Bouy, H., Kolb, J., Marchetti, E., Martín, E. L., Huéamo, N., & Barrado Y Navascués, D. 2008, A&A, **477**, 681
 Buonanno, R., Corsi, C. E., & Fusi Pecci, F. 1989, A&A, **216**, 80
 Campbell, M. A., Evans, C. J., Mackey, A. D., Gieles, M., Alves, J., Ascenso, J., Bastian, N., & Longmore, A. J. 2010, MNRAS, **405**, 421
 Dehnen, W., & Binney, J. J. 1998, MNRAS, **298**, 387
 Dotter, A., et al. 2010, AJ, **708**, 698
 Feltzing, S., & Johnson, R. A. 2002, A&A, **385**, 67
 Ferraro, F. R., et al. 2009, Nature, **462**, 483
 Gao, L., Theuns, T., Frenk, C. S., Jenkins, A., Helly, J. C., Navarro, J., Springel, V., & White, S. D. M. 2010, MNRAS, **403**, 1283
 Gillessen, S., Eisenhauer, F., Trippe, S., Alexander, T., Genzel, R., Martins, F., & Ott, T. 2009, ApJ, **692**, 1075
 Howard, C. D., Rich, R. M., Reitzel, D. B., Koch, A., De Propris, R., & Zhao, H. 2008, ApJ, **688**, 1060
 Johnson, D. R. H., & Soderblom, D. R. 1987, AJ, **93**, 864
 Kuijken, K., & Rich, R. M. 2002, AJ, **124**, 2054
 Lee, Y.-W., Demarque, P., & Zinn, R. 1994, ApJ, **423**, 248
 Lupton, R. H., & Monger, P. 1997, The SM Reference Manual, <http://www.astro.princeton.edu/~rhl/sm/sm.html>
 Magrini, L., Randich, S., Zoccali, M., Jilkova, L., Carraro, G., Galli, D., Maiorca, E., & Busso, M. 2010, A&A, **523**, 11
 Majewska, D. J., Turner, D. G., & Lane, D. J. 2009, MNRAS, **398**, 263
 Marchetti, E., et al. 2007, Messenger, **129**, 8
 Marigo, P., Girardi, L., Bressan, A., Groenewegen, M. A. T., Silva, L., & Granato, G. L. 2008, A&A, **482**, 883
 Minchew, I., Boily, C., Siebert, A., & Bienayme, O. 2010, MNRAS, **407**, 2122
 Mirabel, I. F., Dhawan, V., Mignani, R. P., Rodrigues, I., & Guglielmetti, F. 2001, Nature, **413**, 139
 Momany, Y., Ortolani, S., Bonatto, C., Bica, E., & Barbuy, B. 2008, MNRAS, **391**, 1650
 Momany, Y., et al. 2003, A&A, **402**, 607
 Nakasato, N., & Nomoto, K. 2003, ApJ, **588**, 842
 Ortolani, S., Barbuy, B., & Bica, E. 1995, Messenger, **82**, 20
 Ortolani, S., Bica, E., & Barbuy, B. 1997, MNRAS, **284**, 692
 Ortolani, S., Renzini, A., Gilmozzi, R., Marconi, G., Barbuy, B., Bica, E., & Rich, R. M. 1995, Nature, **377**, 701
 Pfenniger, D. 1984, A&A, **134**, 373
 Pichardo, B., Martos, M., & Moreno, E. 2004, ApJ, **609**, 144
 Press, W. H., Teukolsky, S. A., Vetterling, W. T., & Flannery, B. P. 1992, Numerical Recipes (Cambridge: Cambridge Univ. Press)
 Reid, M. J., & Brunthaler, A. 2004, ApJ, **616**, 872
 Reid, M. J., et al. 2009, ApJ, **700**, 137
 Rey, S.-C., Yoon, S.-J., Lee, Y.-W., Chaboyer, B., & Sarajedini, A. 2001, AJ, **122**, 3219
 Rich, R. M. 1988, AJ, **95**, 828
 Salerno, G., Bica, E., Bonatto, C., & Rodrigues, I. 2009, A&A, **498**, 419
 Sana, H., Momany, Y., Gieles, M., Carraro, G., Beletsky, Y., Ivanov, V. D., de Silva, G., & James, G. 2010, A&A, **515**, A26
 Sandage, A., & Wildey, R. 1967, ApJ, **150**, 469
 Schönrich, R., Binney, J., & Dehnen, W. 2010, MNRAS, **403**, 1829
 Stetson, P. B. 1994, PASP, **106**, 250
 Terndrup, D. M., Popowski, P., Gould, A., Rich, R. M., & Sadler, E. M. 1998, AJ, **115**, 1476
 Terzan, A. 1964a, Haute Prov. Publ., **7**, 2
 Terzan, A. 1964b, Haute Prov. Publ., **7**, 3
 Terzan, A. 1965, Haute Prov. Publ., **8**, 11
 Terzan, A. 1966, Haute Prov. Publ., **8**, 12
 Tiede, G. P., & Terndrup, D. M. 1999, AJ, **118**, 895
 Valenti, E., Ferraro, F. R., & Origlia, L. 2004, MNRAS, **351**, 1204
 Vanhollebeke, E., Groenewegen, M. A. T., & Girardi, L. 2009, A&A, **498**, 95
 Zhao, H. 1996, MNRAS, **283**, 149
 Zoccali, M., Renzini, A., Ortolani, S., Bica, E., & Barbuy, B. 2001, AJ, **121**, 2638

Referências Bibliográficas

- [1] BONNAREL, F.; FERNIQUE, P.; BIENAYMÉ, O.; EGRET, D.; GENOVA, F.; LOUYS, M.; OCHSENBEIN, F.; WENGER, M.; BARTLETT, J. G. The ALADIN interactive sky atlas. A reference tool for identification of astronomical sources. **Astronomy and Astrophysics Supplement Series**, v. 143, p. 33–40, Apr. 2000.
- [2] CLARK, J. S.; NEGUELA, I.; CROWTHER, P. A.; GOODWIN, S. P. On the massive stellar population of the super star cluster Westerlund 1. **Astronomy and Astrophysics**, v. 434, p. 949–969, May 2005.
- [3] CLARK, J. S.; NEGUELA, I.; DAVIES, B.; LARIONOV, V. M.; RITCHIE, B. W.; FIGER, D. F.; MESSINEO, M.; CROWTHER, P. A.; ARKHAROV, A. A. A third red supergiant rich cluster in the Scutum-Crux arm. **Astronomy and Astrophysics**, v. 498, p. 109–114, Apr. 2009.
- [4] DEHNEN, W.; ODENKIRCHEN, M.; GREBEL, E. K.; RIX, H.-W. Modeling the Disruption of the Globular Cluster Palomar 5 by Galactic Tides. , v. 127, p. 2753–2770, May 2004.
- [5] ELMEGREEN, B. G.; EFREMOV, Y. N.; LARSEN, S. A Young Globular Cluster in the Galaxy NGC 6946. **Astrophysical Journal**, v. 535, p. 748–758, Jun. 2000.
- [6] FOK, T. K. T.; NAKASHIMA, J.-I.; YUNG, B. H. K.; HSIA, C.-H.; DEGUCHI, S. Maser Observations of Westerlund 1 and Comprehensive Considerations on Maser Properties of Red Supergiants Associated with Massive Clusters. **Astrophysical Journal**, v. 760, p. 65, Nov. 2012.
- [7] FRIEL, E. D. The Old Open Clusters Of The Milky Way. **Annual Review of Astronomy and Astrophysics**, v. 33, p. 381–414, 1995.

- [8] HEARN, N. C.; LAMB, S. A. Arp 119: A High-Speed Galaxy Collision With Episodic Star Formation. **Astrophysical Journal**, v. 551, p. 651–670, Apr. 2001.
- [9] HIGDON, J. L. Wheels of Fire. I. Massive Star Formation in the Cartwheel Ring Galaxy. **Astrophysical Journal**, v. 455, p. 524, Dec. 1995.
- [10] HODAPP, K.-W. A K' imaging survey of molecular outflow sources. **Astrophysical Journal Supplement Series**, v. 94, p. 615–649, Oct. 1994.
- [11] LADA, C. J.; LADA, E. A. Embedded Clusters in Molecular Clouds. **Annual Review of Astronomy and Astrophysics**, v. 41, p. 57–115, 2003.
- [12] LIN, C. C.; SHU, F. H. On the Spiral Structure of Disk Galaxies. **Astrophysical Journal**, v. 140, p. 646, Aug. 1964.
- [13] MASTROBUONO-BATTISTI, A.; DI MATTEO, P.; MONTUORI, M.; HAYWOOD, M. Clumpy streams in a smooth dark halo: the case of Palomar 5. , v. 546, p. L7, Oct. 2012.
- [14] MERCER, E. P.; CLEMENS, D. P.; MEADE, M. R.; BABLER, B. L.; INDEBETOUW, R.; WHITNEY, B. A.; WATSON, C.; WOLFIRE, M. G.; WOLFF, M. J.; BANIA, T. M.; BENJAMIN, R. A.; COHEN, M.; DICKEY, J. M.; JACKSON, J. M.; KOBULNICKY, H. A.; MATHIS, J. S.; STAUFFER, J. R.; STOLOVY, S. R.; UZPEN, B.; CHURCHWELL, E. B. New Star Clusters Discovered in the GLIMPSE Survey. **Astrophysical Journal**, v. 635, p. 560–569, Dec. 2005.
- [15] MIRABEL, I. F.; DHAWAN, V.; MIGNANI, R. P.; RODRIGUES, I.; GUGLIELMETTI, F. A high-velocity black hole on a Galactic-halo orbit in the solar neighbourhood. **Nature**, v. 413, p. 139–141, Sep. 2001.
- [16] NEGUERUELA, I.; GONZÁLEZ-FERNÁNDEZ, C.; MARCO, A.; CLARK, J. S. A massive association around the obscured open cluster RSGC3. **Astronomy and Astrophysics**, v. 528, p. A59, Apr. 2011.
- [17] NEGUERUELA, I.; GONZÁLEZ-FERNÁNDEZ, C.; MARCO, A.; CLARK, J. S.; MARTÍNEZ-NÚÑEZ, S. Another cluster of red supergiants close to RSGC1. **Astronomy and Astrophysics**, v. 513, p. A74, Apr. 2010.

- [18] ORTOLANI, S.; BARBUY, B.; MOMANY, Y.; SAVIANE, I.; BICA, E.; JILKOVA, L.; SALERNO, G. M.; JUNGWIERT, B. A Fossil Bulge Globular Cluster Revealed by very Large Telescope Multi-conjugate Adaptive Optics. **Astrophysical Journal**, v. 737, p. 31, Aug. 2011.
- [19] PACZYNSKI, B. Are Gamma-Ray Bursts in Star-Forming Regions? **Astrophysical Journal Letters**, v. 494, p. L45, Feb. 1998.
- [20] PIATTI, A. E.; BICA, E.; CLARIA, J. J. Fundamental parameters of the highly reddened young open clusters Westerlund 1 and 2. **Astronomy and Astrophysics Supplement Series**, v. 127, p. 423–432, Feb. 1998.
- [21] REES, R. F.; CUDWORTH, K. M. Did the Globular Cluster NGC 6397 Trigger the Formation of the Young Open Cluster NGC 6231? In: **BULLETIN OF THE AMERICAN ASTRONOMICAL SOCIETY**, v. 35 of **Bulletin of the American Astronomical Society**, p. 1219, Dec. 2003.
- [22] SALERNO, G. M.; BICA, E.; BONATTO, C.; RODRIGUES, I. On the possible generation of the young massive open clusters Stephenson 2 and BDSB 122 by ω Centauri. **Astronomy and Astrophysics**, v. 498, p. 419–423, May 2009.
- [23] SORIA, R.; CROPPER, M. S.; PAKULL, M. W. A ULX in NGC 4559: a “mini-cartwheel” scenario? In: **REVISTA MEXICANA DE ASTRONOMIA Y ASTROFISICA CONFERENCE SERIES**, G. Tovmassian & E. Sion, , editor, v. 20 of **Revista Mexicana de Astronomia y Astrofisica Conference Series**, p. 57–59, Jul. 2004.
- [24] VANDE PUTTE, D.; CROPPER, M. Detecting the effect of globular cluster impacts on the disc of the Milky Way. **Monthly Notices of the Royal Astronomical Society**, v. 392, p. 113–124, Jan. 2009.
- [25] VOROBYOV, E. I. Large-Scale Ring Waves of Star Formation in the Cartwheel Ring Galaxy. **Astronomical and Astrophysical Transactions**, v. 22, p. 95–102, Jan. 2003.
- [26] WALLIN, J. F.; HIGDON, J. L.; STAVELEY-SMITH, L. Dynamically Induced Star Formation in Galaxies from the Passage of Globular Clusters. **Astrophysical Journal**, v. 459, p. 555, Mar. 1996.

- [27] WRIGHT, A. Star Maker. **Nature**, v. 427, p. 207, Jan. 2004.
- [28] ZACHARIAS, N.; FINCH, C. T.; GIRARD, T. M.; HENDEN, A.; BARTLETT, J. L.; MONET, D. G.; ZACHARIAS, M. I. The Fourth US Naval Observatory CCD Astrograph Catalog (UCAC4). **Astronomical Journal**, v. 145, p. 44, Feb. 2013.